Linear analysis of active-medium two-beam accelerator

Miron Voin and Levi Schächter*

Department of Electrical Engineering, Technion–Israel Institute of Technology, Haifa 32000, Israel

(Received 24 March 2015; published 7 July 2015)

We present detailed development of the linear theory of wakefield amplification by active medium and its possible application to a two-beam accelerator (TBA) is discussed. A relativistic train of triggering microbunches traveling along a vacuum channel in an active medium confined by a cylindrical waveguide excites Cherenkov wake in the medium. The wake is a superposition of azimuthally symmetric transverse magnetic modes propagating along a confining waveguide, with a phase velocity equal to the velocity of the triggering bunches. The structure may be designed in such a way that the frequency of one of the modes is close to active-medium resonant frequency, resulting in amplification of the former and domination of a single mode far behind the trigger bunches. Another electron bunch placed in proper phase with the amplified wakefield may be accelerated by the latter. Importantly, the energy for acceleration is provided by the active medium and not the drive bunch as in a traditional TBA. Based on a simplified model, we analyze extensively the impact of various parameters on the wakefield amplification process.

DOI: 10.1103/PhysRevSTAB.18.071302 PACS numbers: 41.75.Lx, 41.75.Jv, 52.38.Kd, 52.40.Mj

I. INTRODUCTION

Classification of a novel acceleration paradigm distinguishes between plasma-based and structure-based schemes. In the former case, a laser or an e-beam pulse injected in plasma generates a space-charge wake that in turn may accelerate electrons or positrons. Both methods have demonstrated gradients of the order 100 GV/m—more than 3 orders of magnitude the operating gradient in existing linear accelerators. However, there are a few other important characteristics (repetition rate, emittance, beam transport, etc.) that are yet to be determined or improved before the plasma-based schemes become a realistic alternative to the International Linear Collider (ILC).

A less drastic change in the acceleration approach is adopted in the structure-based schemes. In this case, an electromagnetic wave is injected or generated inside an electromagnetic structure which is designed to support a TM_{01} mode propagating at the speed of light and whose longitudinal electric field may accelerate electrons or positrons. Several approaches are relevant to the study that follows, therefore we briefly describe them. The compact linear collider (CLIC) [1] is developed at CERN and its essence is to extract *microwave* power from a drive beam (high-current medium-energy) using a periodic metallic structure. This power is injected in a regular, room-temperature, metallic structure which accelerates a low-current high-energy main beam. The two electron beams move along parallel lines which do not coincide. At Argonne National Laboratory (ANL) [2] and Yale University (Omega P) [3] a similar program is pursued except that extraction units consist of a dielectric loaded waveguide—thus the name dielectric wakefield accelerator (DWA). In another configuration of DWA a Cherenkov wake produced by the drive beam traveling along the a dielectric-loaded waveguide may be used to accelerate a trailing beam in the same structure. In this case both drive and accelerated beams move along the *same* axis. The theory of a wakefield in a dielectric-loaded waveguide is presented in Ref. [4].

At *optical* frequencies, Ohm loss makes the metallic acceleration structures irrelevant and they must be replaced by equivalent dielectric structures [5–7]. A general treatment of a wakefield confined by a dielectric structure is given in Ref. [8]. Preliminary results from dielectric acceleration structures driven by laser were recently reported [9], indicating gradients in excess of 0.25 GV/m.

In the present study we propose a novel paradigm that combines two concepts: (i) the well-known two-beam accelerator (TBA) and the recently proposed (ii) enhanced Cherenkov wake amplification by active medium [10]. Its essence is two trains of microbunches propagating along the same axis of a structure that contains *active* medium. In a specific module of the TBA, the first train contains the trigger bunches which generate Cherenkov radiation that in turn is *amplified* by the active medium (AM). Slightly after the medium reaches saturation (L_{sat}), the amplitude of the Cherenkov wake is constant and it is there where we place the trailing train in antiphase with the former such that its bunches are accelerated. In both trains, the spacing between two adjacent microbunches is the resonant wavelength of the medium. By the active medium we mean a medium

*levi@ee.technion.ac.il

FIG. 1. An off-scale schematic of the proposed active-medium two-beam accelerator (AM-TBA) concept. The trigger train in each module generates Cherenkov radiation, which is amplified by the active medium—its amplitude is schematically described by the green line. As this amplification process saturates, the amplitude of the wake is virtually constant and it accelerates the trailing train of bunches.

whose distribution is inverted either electrically or optically. Conceptually, the medium can be solid state or gaseous, though in the specific assessments that follow we consider the latter.

This new scheme, see Fig. 1, is closely related to the coaxial DWA described by Ref. [4] with one principal distinction—the energy required for the acceleration process is not carried by the trigger train, but rather stored in the active medium. Consequently, similar low-current medium-energy beams may be used as both trigger and trailing (accelerated) beams. As already indicated, the role of the former is to generate initial Cherenkov radiation which will be amplified by the active medium and then accelerate the latter. Typically, in the trailing beam there are order of a few 10^6 electrons and the gradient is of the order of 1 GV/m. For satisfying the luminosity requirements, the electrons must reach the interaction point at a rate of 10^{14} electrons per second [11]. Consequently, the repetition rate of the system must be of about 100 MHz corresponding to 3 m spacing between two consecutive trailing trains. Energy wise, considering a 1 m long module, the total energy the train absorbs is 0.1 mJ thus assuming 10% conversion efficiency the active medium should contain at least 1 mJ in each one meter long module. Whatever optical energy is lost, it has to be replenished within 10 nsec such that the next trigger train of bunches experiences the same conditions. In the rough assessment from the above, it was tacitly assumed that the saturation length is negligible comparing to the spacing between two consecutive trigger trains—for the characteristic values to be discussed subsequently, $L_{\mathrm{sat}} \sim 2$–10 cm.

It warrants clarifying here that we use the word train in two different contexts: (i) at the single module level, we have the train of trigger microbunches and train of trailing (accelerated) microbunches. The spacing between the two microtrains is of the order of the saturation length (centimeters). (ii) At the system level we have two trains. One contains all the trigger microtrains and the other consists of all the trailing microtrains. The spacing between two macrotrains is determined by the repetition rate of the laser (meters).

Figure 2 shows a schematic of a single module. The vacuum channel, where the electrons propagate, is confined

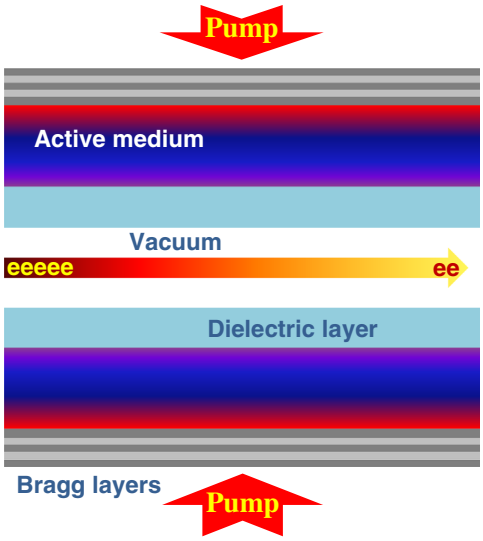

FIG. 2. Schematic (not in scale) of the conceived configuration. The vacuum tunnel facilitates smooth transport of electrons. Between the high vacuum region and the pressurized active gas there is a low-loss thick dielectric vessel designed to withstand the pressure gradient. The active medium is confined by a Bragg structure designed to confine an evanescent field but transfer propagating waves. A pulsed CO_2 laser (not shown) excites a CO_2 based mixture from the outside the Bragg waveguide, ensuring uniform population inversion.

by a relatively thick dielectric layer designed to sustain the high pressure gas mixture which consists the active medium. As the only role of the dielectric layer is to provide a vacuum channel in a gaseous active medium, in case the latter is solid (NdYAG) no dielectric layer would be required. The ultrarelativistic electron beam passing the vacuum channel polarizes both the dielectric and the active medium triggering in *both* a Cherenkov wake which will propagate through the structure with velocity of the triggering beam. The whole structure may be designed in such a way that one of the eigenfrequencies of the triggered wake is equal to the resonant frequency of the active medium. The analysis that follows shows that this resonant mode will be amplified by the active medium. A part of the amplified Cherenkov radiation will propagate through the vacuum channel behind the triggering beam with phase velocity equal to that of the trigger and may be used to accelerate trailing beam branches. The active medium and the Cherenkov wake are confined by the Bragg waveguide. In spite that it confines the Cherenkov radiation generated by the electrons, the Bragg waveguide facilitates full transfer of optical energy to ensure population inversion of the mixture of gases. While detailed design of the confining Bragg structure is beyond the scope of this study, a good example of such design may be found in Ref. [7]. For instance, in a case of a CO_2 mixture as an active medium, the structure may be engineered to confine the 10.6 μm Cherenkov wake and to be transparent for

pumping radiation at 4.2 μm from an HBr laser [12] or 3.5–4.0 μm from a DF laser [13]. For NdYAG the corresponding numbers are 1.06 μm and 808 or 812 nm. Throughout this study we are biased by the assumption that the active medium is gaseous (CO_2) since we assume that it will be easier to make micrometer long microbunches than submicrometer; however, by no means do we rule out the possibility of solid-state active medium.

In the present study, we bring a detailed account of the concept briefly introduced in [10]. First the essence of the concept is described in details on the basis of a simplified model. In the latter the electrons are allowed to move freely through the active medium without a need to account for presence of the vacuum channel and the solid dielectric surrounding it. Another departure of the simplified model from the reality is that the confining Bragg structure is replaced with an ideal metal wall. The absolute value of the reflection coefficient for the frequency of interest from a metallic surface or a Bragg mirror is close to unity in both cases, while the phase of the reflected wave is different. Obviously in a detailed design this phase difference should be accounted for by proper selection of the structure geometry, but it is beyond the scope of the present conceptual study. In Sec. II we summarize the main positions of our simplified model for wake amplification by active medium. Section III provides formalism for power exchange in the structure. Section IV determines the main parameters for a specific active medium. Section V is devoted to impact of various parameters on the wake amplification. In Sec. VI we provide simulation results for wake amplification with some geometry optimization for two different pressure levels of the gaseous medium. In the context of this study simulation is a numerical evaluation of analytical results. In Sec. VII we return to the realistic configuration shown schematically in Fig. 2, presenting a mathematical model for wake dynamics and power considerations.

II. SIMPLIFIED MODEL

In [10] we have briefly considered a simplified model in order to emphasize the physical essence of the paradigm. In the present study we show a more detailed analysis based on that model and improve the latter in an attempt to make the assessments more realistic. Explicitly, we have demonstrated that operation close to the cutoff of Cherenkov radiation results in an *enhanced* gain. In the framework of the simplified model, the Bragg waveguide is replaced by a metallic waveguide ignoring for simplicity's sake Ohm loss and the way the medium is excited; its radius is denoted by R_w. Further, we ignore the small-angle scattering effect of the gaseous medium on both trigger and accelerated electrons, therefore the dielectric layer that buffers between the vacuum tunnel and the active medium is ignored such that the electrons propagate freely in the active medium.

An assessment of the gain enhancement can be performed in three steps: *first* we observe that assuming lossless wall, a discrete spectrum of Cherenkov eigenfrequencies $\omega_s = (cp_s/R_w)(\varepsilon_r - \beta^{-2})^{-1/2}$ is generated; here p_s are the zeros of the Bessel function of the zero order and first kind $J_0(p_s) \equiv 0$; $s = 1, 2, \ldots, \infty$, $\varepsilon_r > 1$ is the (frequency independent) dielectric coefficient in the *absence* of the active medium and β is the normalized velocity of the charged particle. In the ultrarelativistic regime ($\gamma \to \infty$) the Cherenkov slippage

$$\bar{\varepsilon} \equiv \varepsilon_r - \beta^{-2} \simeq \varepsilon_r - 1 \tag{1}$$

is virtually independent of the energy of the electrons. *Second*, assuming a linear regime, the active medium is described by

$$\varepsilon(\omega) = \varepsilon_r + \frac{\omega_p^2}{\omega_0^2 + j\omega\Delta\omega + (j\omega)^2}, \tag{2}$$

where ω_0 is the resonance of the medium, $\Delta\omega$ is its bandwidth, $\omega_p^2 = -2c\alpha\Delta\omega\sqrt{\varepsilon_r}$ and α is the gain per unit length. The expression for ω_p^2 is derived from a consideration that gain α for a plane wave at resonance equals the gain associated with the imaginary component of the wave vector. *Third*, we design the parameters such that there is only one eigenmode ($s = s_0$) whose eigenfrequency ($\omega_{s=s_0}$) virtually equals the resonant frequency of the medium (ω_0), namely $\omega_{s_0} \simeq \omega_0$. This eigenmode will be amplified by the active medium—*similar* to a TEM mode. We emphasize similar and not identical since, in the Cherenkov case, the phase and group velocities are determined by the trigger bunch velocity. Consequently, the amplification occurs both in space and in time. In the case of a laser, both velocities are determined by the medium and the amplification may occur in space (amplifier) or in time (oscillator due to reflections). In the latter case, the medium and the boundary conditions impose the growth rate.

A. Kinematics

In the presence of the active medium, the eigenresonances, associated with the bunch-medium interaction, are a solution of a fourth order polynomial, rather than second order in its absence, and the dominant of the four modes are given by

$$\omega_\pm = \omega_0 + j\frac{\Delta\omega}{4}(1 \pm \sqrt{1 + 16a^2}) \equiv \omega_0 + j\delta\omega_\pm \tag{3}$$

wherein $a^2 \equiv c\alpha/2\bar{\varepsilon}\Delta\omega$; for example, if $\Delta\omega \simeq 2\pi \times 37 \times 10^9$, $\bar{\varepsilon} = 1.42 \times 10^{-3}$ and $\alpha = 1\ \mathrm{m}^{-1}$, then $a \simeq 0.674$. This analytic expression clearly reveals the effect of the Cherenkov "slippage" factor $\bar{\varepsilon}$ on the enhancement process explicitly, $\delta\omega_\pm = (\Delta\omega/4)(1 \pm \sqrt{1 + 8c\alpha/\bar{\varepsilon}\Delta\omega})$ and at the

limit $\bar{\varepsilon} \to 0$ the Cherenkov wake is close to its "cutoff" and consequently, the growth rate of the wake is very large.

B. Dynamics

To each one of the eigenfrequencies corresponds an eigenmode, and in what follows we establish the wake in terms of these modes in two dimensions (r, z) as well as in time defining $\tau \equiv t - z/\mathrm{v}$. We start with the exact expression for the longitudinal electric field given the current density $J_z(r,z,t) = -(q\mathrm{v}/2\pi r)\delta(r - r_\sigma)\delta(z - z_\sigma - \mathrm{v}t)$ namely,

$$E_z^{(s,\sigma)}(r,\tau) = \frac{q}{4\pi^2\varepsilon_0\varepsilon_\mathrm{r}}\sum_s G_s(r,r_\sigma) \times \int_{-\infty}^{\infty} d\omega j\omega F_s(\omega)\exp\left[j\omega\left(\tau + \frac{z_\sigma}{c\beta}\right)\right]. \tag{4}$$

Note that q is the charge of an infinitesimally thin loop of radius r_σ which at $t = 0$ is located at $z = z_\sigma$ and

$$F_s(\omega) \equiv \frac{1 - \frac{1}{\varepsilon(\omega)\beta^2}}{c^2\frac{p_s^2}{R_\mathrm{w}^2} - [\varepsilon(\omega) - \frac{1}{\beta^2}]\omega^2} \simeq \frac{1}{\varepsilon_\mathrm{r}}\frac{\omega_0^2 + j\omega\Delta\omega - \omega^2}{(\omega_{\mathrm{C,s}}^2 - \omega^2)(\omega_0^2 + j\omega\Delta\omega - \omega^2) - \omega_{\mathrm{C,p}}^2\omega^2}, \tag{5}$$

where $\omega_{\mathrm{C,s}}^2 \equiv c^2 p_s^2/R_\mathrm{w}^2\bar{\varepsilon}$ and $\omega_{\mathrm{C,p}}^2 \equiv \omega_\mathrm{p}^2/\bar{\varepsilon}$. The former determines the poles of longitudinal Green's function, whereas $G_s(r,r') \equiv J_0(p_s r/R_\mathrm{w})J_0(p_s r'/R_\mathrm{w})[R_\mathrm{w}^2 J_1^2(p_s)/2]^{-1}$ is the radial component of Green's function. In the approximation of Eq. (5) we had ignored the poles associated with the dielectric alone, $\varepsilon(\omega) = 0$.

Based on this formulation, we demonstrated in [14] that the eigenfrequencies are exact expressions subject to the assumptions made and had shown that the *interacting mode* $(s = s_0)$ satisfies

$$E_z^{(s_0,\sigma)}\left(r, \tau + \frac{z_\sigma}{c\beta}\right) = \frac{q}{2\pi\varepsilon_0\varepsilon_\mathrm{r}}G_{s_0}(r,r_\sigma)U\left(\tau + \frac{z_\sigma}{c\beta}\right), \tag{6}$$

where

$$U(\tau) \equiv \frac{h(\tau)}{\delta\omega_+ - \delta\omega_-} \times \left\{ \begin{matrix} \frac{\delta\omega_-\delta\omega_+}{\omega_0}\sin(\omega_0\tau)\begin{bmatrix}\exp(-\delta\omega_+\tau) \\ -\exp(-\delta\omega_-\tau)\end{bmatrix} \\ +\cos(\omega_0\tau)\begin{bmatrix}\delta\omega_+\exp(-\delta\omega_-\tau) \\ -\delta\omega_-\exp(-\delta\omega_+\tau)\end{bmatrix}\end{matrix}\right\}. \tag{7}$$

As the $\delta\omega_-, \delta\omega_+ \ll \omega_0$, components of $U(\tau)$ proportional to $\sin(\omega_0\tau)$ are negligible, while from the two remaining components only one, proportional to $\exp(-\delta\omega_-\tau)$, is growing in τ. Thus, many resonance wavelengths behind the trigger bunch $(\tau c/\lambda_0 \gg 1)$, the field dynamics may be approximated as

$$U(\tau) \simeq \frac{\delta\omega_+}{\delta\omega_+ - \delta\omega_-}\cos(\omega_0\tau)\exp(-\delta\omega_-\tau) \tag{8}$$

clearly revealing the exponentially growing character of the wake $(\delta\omega_- < 0)$. For reasons that will become clear subsequently, it is important to notice that $U(0) = 1/2$.

III. POWER CONSIDERATIONS

A. Trigger bunch

With the single-particle wake established, we may now proceed to evaluation of the power generated by a train of microbunches of a given transverse $f_\perp(r)$ and longitudinal $f_\parallel(z)$ distributions. For our present purposes, we may assume that the two distributions are statistically independent—without any loss of generality. Formally, the power generated by a current density as determined prior to Eq. (4) is given by $P^{(\mathrm{spo})} = \int dV J_z(r,z,t)E_z^{(s_0,\sigma)}(r,z,t)$ thus, $P^{(\mathrm{spo})} = (q^2\mathrm{v}/2\pi\varepsilon_0\varepsilon_\mathrm{r})\sum_\sigma G_{s_0}(r_\sigma, r_\sigma)U(0)$. As indicated above, $U(0) = 1/2$ and using the definition of the radial Green's function the noncoherent component of the power generated by N_el electrons in the resonant mode is

$$P^{(\mathrm{spo})} = \frac{-N_\mathrm{el}q^2\mathrm{v}}{4\pi\varepsilon_0\varepsilon_\mathrm{r}R_\mathrm{w}^2}\frac{2}{J_1^2(p_{s_0})}F_\perp^{(\mathrm{spo})} \tag{9}$$

wherein $F_\perp^{(\mathrm{spo})} \equiv 2\pi\int_0^{R_\mathrm{w}} drrf_\perp(r)J_0^2(p_{s_0}r/R_\mathrm{w})$ is the transverse spontaneous form factor.

For assessment of the *coherent* component of the power, we recall that the current density associated with the ensemble is $J_z(r,z,t) = -(q\mathrm{v}/2\pi r)\sum_\sigma\delta(r - r_\sigma)\times\delta(z - z_\sigma - \mathrm{v}t)$ implying that the wakefield $E_z^{(s_0)}(r,z,t) = (q/2\pi\varepsilon_0\varepsilon_\mathrm{r})\sum_\sigma G_{s_0}(r,r_\sigma)U[t - (z - z_\sigma)/c\beta]$; the coherent component of the power is $P^{(\mathrm{coh})} = \int dV J_z(r,z,t)\times E_z^{(s_0)}(r,z,t) - P^{(\mathrm{spo})}$; therefore the coherent power is

$$P^{(\mathrm{coh})} = \frac{-N_\mathrm{el}q^2\mathrm{v}}{4\pi\varepsilon_0\varepsilon_\mathrm{r}R_\mathrm{w}^2}(N_\mathrm{el} - 1)\frac{2}{J_1^2(p_{s_0})}F_\perp^{(\mathrm{coh})}F_\parallel^{(\mathrm{coh})} \tag{10}$$

wherein $F_\perp^{(\mathrm{coh})} \equiv [2\pi\int_0^{R_\mathrm{w}} drrf_\perp(r)J_0(p_{s_0}r/R_\mathrm{w})]^2$ is the coherent transverse form factor, whereas $F_\parallel^{(\mathrm{coh})} \equiv 2\int_{-\infty}^{\infty} dzf_\parallel(z)\int_{-\infty}^{\infty} d\zeta f_\parallel(\zeta)U[(z - \zeta)/c\beta]$ represents the longitudinal counterpart.

Finally, the total power emitted

$$P^{(\mathrm{tot})} = \frac{-N_\mathrm{el}q^2\mathrm{v}}{4\pi\varepsilon_0\varepsilon_\mathrm{r}R_\mathrm{w}^2}[F_\perp^{(\mathrm{spo})} + (N_\mathrm{el} - 1)F_\parallel^{(\mathrm{coh})}F_\perp^{(\mathrm{coh})}]. \tag{11}$$

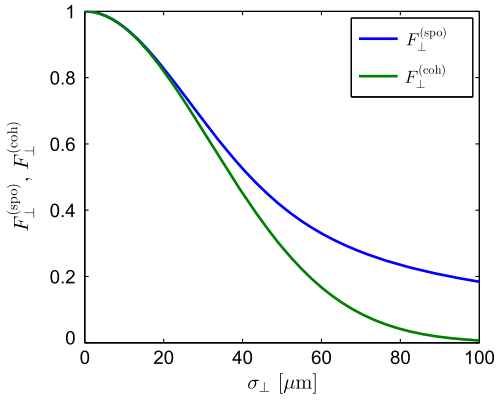

FIG. 3. Spontaneous $F_\perp^{(spo)}$ and coherent $F_\perp^{(coh)}$ transverse form factors for a Gaussian transverse distribution as functions of the rms value $\sigma_\perp$ for $s_0 = 355$ and $R_w = 50$ mm.

Assuming transverse distribution to be Gaussian and characterized by rms value $\sigma_\perp$, namely $f_\perp(r) = (1/2\pi\sigma_\perp^2)\exp(-r^2/2\sigma_\perp^2)$ and assuming $R_w \gg \sigma_\perp$ we may approximate the transverse form factors by semi-indefinite integrals having analytical solutions, which with definition $\bar{\sigma}_\perp \equiv p_{s_0}\sigma_\perp/R_w$ read

$$F_\perp^{(spo)} \simeq \frac{1}{\sigma_\perp^2}\int_0^\infty dr r \exp\left(-\frac{r^2}{2\sigma_\perp^2}\right) J_0^2\left(p_{s_0}\frac{r}{R_w}\right) = \exp(-\bar{\sigma}_\perp^2) I_0(\bar{\sigma}_\perp^2) \quad (12)$$

$$F_\perp^{(coh)} \simeq \left[\frac{1}{\sigma_\perp^2}\int_0^\infty dr r \exp\left(-\frac{r^2}{2\sigma_\perp^2}\right) J_0\left(p_{s_0}\frac{r}{R_w}\right)\right]^2 = \exp(-\bar{\sigma}_\perp^2). \quad (13)$$

Solution for integrals in Eq. (12) and (13) may be found in [15], Eq. (10.22.67). In Fig. 3 we present spontaneous and coherent transverse form factors as a function of the transverse distribution rms value for $s_0 = 355$ and $R_w = 50$ mm.

As in the case of transverse form factors we expect the longitudinal distribution of a single microbunch to be close to a Gaussian characterized by rms value $\sigma_\parallel$. Longitudinal form factor $F_\parallel^{(coh)}$ is calculated numerically for 10 atm active medium values summarized in Table I and the resulting function is presented in Fig. 4. A rough analytic estimation of the form factor $F_\parallel^{(coh)}$ is presented in Appendix A.

It shall be emphasized that we had considered in this section only resonant mode s_0. In reality, the contribution of other modes in the near field *is not* negligible; consequently, the superposition of modes shall be taken into account for an accurate estimate of the power exchange.

TABLE I. Simulation parameters.

Parameter		Value
Medium (CO_2)		
Resonance wavelength	λ_0	10.6 μm
Resonance frequency	ω_0	1.78×10^{14} rad/s
Resonance bandwidth	$\Delta\omega$	4.62×10^{10} rad/s (@∼2 atm)
		2.32×10^{11} rad/s (@∼10 atm)
Growth rate coefficient	α	1 m^{-1}
Relative permittivity	ε_r	1.00028 (@∼2 atm)
		1.00142 (@∼10 atm)
Waveguide		
Radius	R_w	50 mm
Resonance mode	s_0	158 (@∼2 atm)
		355 (@∼10 atm)
e-beam		
Lorentz factor	γ	600
Total charge	Q_{total}	10^9 *e*
Length	L_{tr}	150 λ_0
Modulation	A_m	0.2
Radius (rms)	σ_b	30 μm

B. Far field

Several thousands of λ_0 behind the trigger bunch the resonant mode dominates the wakefield and the amplitude of the longitudinal electric field may be approximated by this resonant mode only. For an ultrarelativistic triggering bunch of length $L_t \gg \lambda_0$ density modulated at the medium resonance frequency with depth A_m, while $A_m = 1$ means 100% modulation depth, the amplitude of the wake many wavelengths behind the trigger is approximated as

$$|E_z^{(s_0)}(\tau, L_t, A_m)| \simeq E_z^{(s_0,\sigma)}(0)\frac{1+(1+16a^2)^{-1/2}}{2} \times \exp(-\delta\omega_-\tau)\frac{|\delta\omega_-|}{\omega_0}F^{(mod)}, \quad (14)$$

where

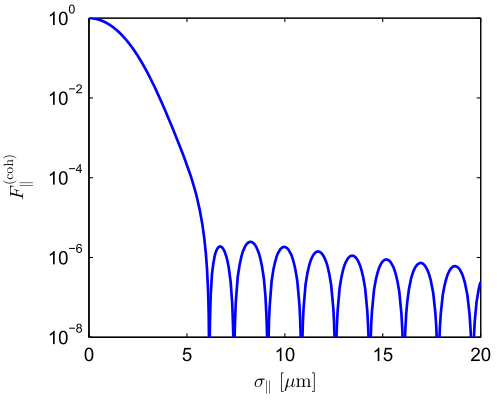

FIG. 4. Coherent longitudinal form factor $F_\parallel^{(coh)}$ for a Gaussian longitudinal distribution as a function of the rms value $\sigma_\parallel$ for 10 atm active medium values summarized in Table I.

$$F^{(\mathrm{mod})} \equiv \frac{\omega_0}{|\delta\omega_-|}\frac{1-\exp(-2\pi N_\lambda \frac{|\delta\omega_-|}{\omega_0})}{2\pi N_\lambda} \times \begin{cases} 1 & A_m = 0 \\ \frac{A_m}{2}\frac{\omega_0}{|\delta\omega_-|} & A_m \sim 0.1 \end{cases}. \quad (15)$$

Here N_λ is the length of the modulated trigger bunch, expressed in the medium resonance wavelengths. A derivation of expression (14) is shown in Appendix B. This approximation is in agreement with simulation results shown in Sec. VI. The factor $F^{(\mathrm{mod})}$ is accounting for the contribution of the bunch's finite length and its modulation. For a zero bunch modulation ($A_m = 0$) and for short bunches ($N_\lambda \to 0$) this factor approaches its maximum value of unity. One would expect the field to be identically zero for $L_t > \lambda_0$ at $A_m = 0$, but the amplification ($\delta\omega_- < 0$) along the bunch length prevents exact compensation of the field produced by the bunch charge along wavelength λ_0. On the other hand, for significant modulation values ($A_m \sim 0.1$) the contribution of the bunch's finite length and its modulation is limited by the maximum value of $A_m/2$ and gradually degrades toward zero with increase of the bunch length N_λ.

IV. MEDIUM PARAMETERS

So far no attempt has been made to optimize the active medium for our purposes. While solid-state lasers have a clear advantage of relatively high efficiency, the CO_2 laser has the inherent advantage of long wavelength, making the bunch generation much easier. A more pragmatic reason for our choice of a CO_2 based mixture is the future feasibility of testing the concept at BNL-ATF. In the present section, we consider the parameters of the active medium or more specifically, we estimate realistic values for the parameters of Eq. (2) for a CO_2 mixture.

It should be pointed out that while we focus here on CO_2 active medium, most arguments hold for other gaseous media (HeNe, Ar^+, Kr, Xe or excimer). While the CO_2 has a variety of resonances, the dominant corresponds to 10.6 μm wavelength or $\omega_0 = 1.78 \times 10^{14}$ rad/s; the remaining parameters are inferred based on proven laser systems—BNL [17] and UCLA [18] and other sources, referenced comprehensively in our past publications [10] and [14]. In particular, for pressure of 10 atm, small-signal gain with respect to the intensity at resonance is estimated as $\alpha = 1\ \mathrm{m}^{-1}$, effective bandwidth of the active spectral line as $\Delta\omega_{\mathrm{eff}} \simeq 2\pi \times 37$ GHz and dielectric coefficient ε_r for the $CO_2:N_2:He$ (1:1:14) mixture is taken to be $\varepsilon_r - 1 \simeq 1.42 \times 10^{-3}$. Note that closely located 10R as well as 9P and 9R branches of CO_2 spectral lines may affect significantly relative dielectric coefficient value at 10.6 μm. We should keep in mind that for a realistic configuration a "fine-tuning" of the mixture will be required in order to achieve desirable ε_r value at the wavelength of interest.

V. PARAMETRIC DEPENDENCE

Our goal in this section is to estimate general trends of the wakefield amplification dependence on main parameters of the active medium. First we want to evaluate these parameters assuming them to be independent variables, although it is not the case for an actual system, as will be shown subsequently, as virtually all of them depend on the pressure. The specific pressure value will depend on constrains of a chosen operation regime. In this study we chose to consider two pressure values—2 and 10 atm.

Dependence on the resonant wakefield mode amplitude on main parameters of the medium $2000\lambda_0$ behind the trigger found from Eq. (14) are shown in Fig. 5 by dashed lines. For comparison results from the full simulation taking in account 1000 modes of the wake are shown by circles on the same graph. Two trends are evident: first, increasing the bandwidth by a (magnification) factor $M = 2$ leads to an order of magnitude increase in the gradient whereas a similar magnification of the gain leads to increase of more than 2 orders of magnitude in the gradient. Note that the gradients above 10 GV/m should be considered only as indicators since breakdown and saturation will limit the electric field to this level. The second important trend is the slippage effect. Enhancing the slippage by a factor of $M = 2$ leads to more than an order of magnitude reduction in the gradient.

A. Pressure

In Fig. 5 the three parameters were assumed to be independent. In practice, they are dependent and the pressure affects them all. In what follows we develop a relatively simple model that will allow us to make a more reliable, self-consistent assessment of the gradient

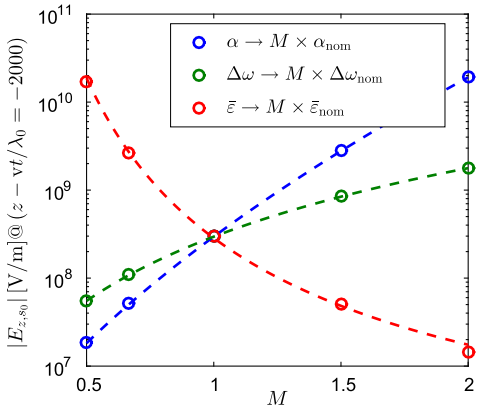

FIG. 5. Dependency on the resonant wakefield mode amplitude on main parameters of the medium (α, $\Delta\omega$ and $\bar{\varepsilon} \equiv \varepsilon_r - \beta^{-2}$) at $2000\lambda_0$ behind the trigger found from Eq. (14) (dashed lines). Results from the full simulation taking in account 1000 modes are shown by circles. Nominal values for the parameter are corresponding to values in Table I for 10 atm.

assuming that the geometrical parameters are kept constant. Our starting point is to assume the pressure broadening to be a dominant mechanism affecting the spectral linewidth and the $\Delta\omega$ to be proportional to the gas mixture pressure. The UCLA group assumes in [18] the CO_2 spectral linewidth to be 37 GHz at 10 atm due to pressure broadening for the $CO_2:N_2:He$ (1:1:14) mixture. Explicitly this assumption may be formulated as

$$\Delta\omega(P) = 2\pi g_P P. \tag{16}$$

Consequently, the pressure broadening coefficient for the mixture is estimated as $g_P = 3.7$ GHz/atm. This value is of the same order of magnitude as the pressure broadening values for CO_2 spectral lines from the HITRAN database [19], where for the 10.6 μm (944.2 cm^{-1}) spectral line pressure self-broadening and air broadening are specified as 5.88 GHz/atm and 4.30 GHz/atm (FWHM values).

The growth rate coefficient α is related to population difference density Δn as

$$\alpha = \frac{1}{2}\frac{\lambda_0^2}{2\pi}\frac{A_{21}}{\Delta\omega}\Delta n, \tag{17}$$

where Einstein's A coefficient $A_{21} \simeq 0.2\ s^{-1}$ for CO_2 spectral lines according to [19] and the sign of Δn is positive for inverted population. Thus knowing α and $\Delta\omega$ we can estimate the population difference density and in our case

$$\Delta n = 4\pi\frac{\alpha\Delta\omega}{\lambda_0^2 A_{21}} \simeq 1.300\times 10^{23}\ m^{-3}. \tag{18}$$

The density of CO_2 molecules at a pressure of 10 atm and at room temperature for $CO_2:N_2:He$ (1:1:14) mixture is

$$n_{CO_2} \simeq 1.48\times 10^{25}\ m^{-3}. \tag{19}$$

The *relative population difference density* is

$$\Delta\bar{n} \equiv \frac{\Delta n}{n_{CO_2}} \simeq 0.88\%. \tag{20}$$

It was shown by Siegman [20] that for a "good laser system" the pressure-dependent nonradiative decay rates may be neglected for a rough assessment of the relative population difference density and for a four-level system the latter is estimated as

$$\frac{\Delta n}{n_0} \equiv \Delta\bar{n} \simeq \frac{\eta W_p \tau_{rad}}{1+\eta W_p \tau_{rad}}. \tag{21}$$

Here Δn is an absolute population difference density, n_0 is the total density of the molecules or atoms, η is the fluorescence quantum efficiency, W_p is a pumping rate associated with pumping transition probability and τ_{rad} is a reciprocal of the radiative decay rate for the active transition of the medium—see Appendix C for details.

Assuming that for a realistic laser mixture, from which our parameters are taken, η is on the order of unity, we may estimate that the relative population difference density $\Delta\bar{n}$ is approximately constant over pressure as long as mixture proportions are unchanged. Then expressing the growth rate coefficient α in terms of $\Delta\bar{n}$ and substituting expression for $\Delta\omega$ we find

$$\alpha(P) = \frac{1}{2}\frac{\lambda_0^2}{2\pi}\frac{A_{21}}{(2\pi g_P P)}\left(\frac{1}{1+1+14}\frac{P}{k_B T}\right)\Delta\bar{n}. \tag{22}$$

The assumption that the relative population difference density $\Delta\bar{n}$ is independent of pressure makes the growth rate coefficient α defined by Eq. (22) independent of pressure as well. If for a particular gas mixture $\Delta\bar{n}$ would show some pressure dependence, it may be easily taken into account. For what follows we will consider $\alpha(P) = \text{const}$.

Based on Lorentz-Lorenz equation electric susceptibility $(\varepsilon_r - 1)$ is proportional to the pressure and since $\varepsilon_r(P) = 1 + f_P P$ we have

$$\bar{\varepsilon}(P) = f_P P - \frac{1}{\gamma^2 - 1} \simeq f_P P - \gamma^{-2}; \tag{23}$$

for our parameters $f_P = 1.42\times 10^{-4}\ atm^{-1}$.

We now may express an effective enhanced gain as a function of pressure

$$\alpha_{eff}(P) = -\frac{\Delta\omega}{4c}\left(1-\sqrt{1+\frac{8}{\bar{\varepsilon}}\frac{c\alpha}{\Delta\omega}}\right) \simeq -\frac{2\pi g_P P}{4c}\left(1-\sqrt{1+\frac{4}{\pi}\frac{c\alpha}{f_P g_P P^2}}\right). \tag{24}$$

It is important to keep in mind that expression (24) is valid only for values of pressure satisfying the resonance condition $\omega_0 = (c p_s/R_w)\bar{\varepsilon}^{-1/2}$ and the latter is affected by pressure via $\bar{\varepsilon}(P)$. If we assume the waveguide radius R_w is unchanged, the resonance condition is satisfied for "discrete" values of pressure $P(s_0)$ defined by

$$p_{s_0} = 2\pi\frac{R_w}{\lambda_0}\sqrt{\bar{\varepsilon}[P(s_0)]} \tag{25}$$

consequently, the pressure values satisfying the resonance condition are

$$P(s_0) = \frac{\left(\frac{p_{s_0}}{2\pi}\frac{\lambda_0}{R_w}\right)^2 + \frac{1}{\gamma^2-1}}{f_P} \simeq \frac{\left(\frac{s_0-1/4}{2}\frac{\lambda_0}{R_w}\right)^2 + \gamma^{-2}}{f_P}. \quad (26)$$

In the last expression we took in account that the roots of the zero-order Bessel function of the first kind may be approximated as $p_s(s) \simeq \pi s - \pi/4$; thus, the dependence of the resonant mode on the pressure may be expressed as

$$s_0(P) \simeq \text{Integer}\left(\frac{1}{4} + 2\frac{R_w}{\lambda_0}\sqrt{f_P P - \gamma^{-2}}\right). \quad (27)$$

From here the minimal pressure value for our set of parameters is $P_1 \simeq 0.0196$ atm, and the pressure "resolution" required in order to distinguish between different modes s is

$$\Delta P(s_0) \simeq \frac{s_0}{2f_P}\left(\frac{\lambda_0}{R_w}\right)^2 \quad (28)$$

thus, if $s_0 = 360$, then $\Delta P(360) \simeq 0.05$ atm.

Let us summarize the effects of the gas mixture pressure in short: as the pressure directly affects the mixtures permittivity, namely $\varepsilon_r - 1 \propto P$, for an ultrarelativistic beam the Cherenkov slippage factor $\bar{\varepsilon}$ is also proportional to the pressure, Eq. (23), thus making the squared eigenfrequencies of the wake to be inversely proportional to the pressure ($\omega_{C,s}^2 \equiv c^2 p_s^2/R_w^2\bar{\varepsilon}$). Spectral linewidth is directly proportional to the pressure and finally the enhanced gain depends on pressure as shown by Eq. (24). In the next sections we will show the complex effect of the pressure on the wake growth rate. As the relative population difference density is expected to be constant, the absolute population difference density is directly proportional to the pressure, which makes an estimated saturation of squared electric field of the wake to be directly proportional to the pressure as well.

B. Energy spread

Assessment for the enhanced gain, Eq. (24), is based on assumption that the resonance condition $\omega_{s_0} = \omega_0 = (cp_s/R_w)\bar{\varepsilon}^{-1/2}$ is perfectly matched for a given energy of the triggering bunch. In reality, there is a certain spread in the bunch energy resulting in some "detuning" from the resonance for each electron. In order to take this into account we assume the Lorentz factor γ to be normally distributed with a standard deviation $\Delta\gamma$ and an expectation value γ_0:

$$f_\gamma(\gamma) = \frac{1}{\sqrt{2\pi}\Delta\gamma}\exp\left[-\frac{(\gamma-\gamma_0)^2}{2\Delta\gamma^2}\right]. \quad (29)$$

In practice, the growth rate coefficient α is in general frequency dependent and for a case when the pressure broadening is dominant this dependency is approximated by a Lorentzian line shape [21]

$$\alpha(\omega) = \pi\alpha_0(\Delta\omega/2)\left[\frac{1}{\pi}\frac{\Delta\omega/2}{(\omega-\omega_0)^2 + (\Delta\omega/2)^2}\right] \quad (30)$$

and an averaged effective enhanced gain for a wake generated by the energy distributed triggering bunch may be calculated from

$$\frac{E_z(L)}{E_0} = \int_{-\infty}^{\infty} d\gamma f_\gamma(\gamma)\exp[\alpha_{\text{eff}}(\gamma)L] \equiv \exp(\langle\alpha_{\text{eff}}\rangle L) \quad (31)$$

or explicitly

$$\langle\alpha_{\text{eff}}\rangle = \frac{1}{L}\ln\left\{\int_{-\infty}^{\infty} d\gamma f_\gamma(\gamma)\exp\left[\alpha_{\text{eff}}(\gamma)L\right]\right\}. \quad (32)$$

We calculated $\langle\alpha_{\text{eff}}\rangle$ from Eq. (32) numerically for $\gamma_0 = 600$ and $\Delta\gamma/\gamma_0 = 0.001$. The results are presented in Fig. 6.

As the Cherenkov slippage approaches zero at low pressures, the gain for a wake produced by particles with the energy satisfying the resonance condition exactly, grows by an order of magnitude. However, due to the energy spread of the particles at the pressure values below 0.5 atm a significant part of the triggering bunch produces wake out of resonance reducing the average gain for the wake. At the same time for pressure values well above 0.5 atm the energy spread of $\Delta\gamma/\gamma_0 = 0.001$ has virtually no effect on the average gain; with pressure, the value of $\langle\alpha_{\text{eff}}\rangle$ approaches asymptotically the curve corresponding to $\Delta\gamma = 0$. The effective gain, defined by Eq. (31), depends on the distance L behind the trigger bunch and on the degradation due to low pressure; the latter is less prominent for large values of L. In other words, $\langle\alpha_{\text{eff}}\rangle$ approaches the curve corresponding to $\Delta\gamma = 0$ for large values of L. We need to keep in mind that present assessment does not take

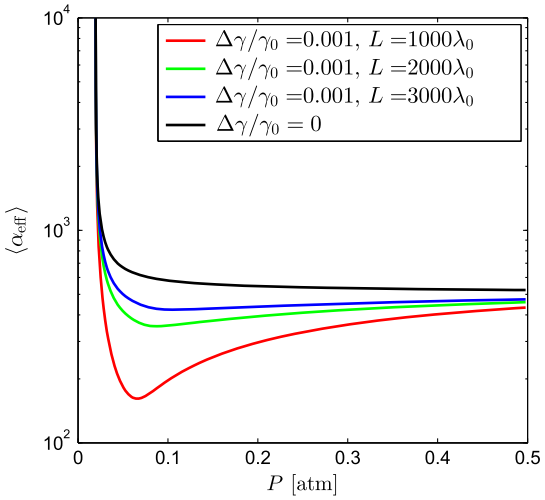

FIG. 6. Averaged effective enhanced gain for triggering bunch distribution $\Delta\gamma/\gamma_0 = 0.001$ at different distances L behind the triggering bunch and for $\Delta\gamma/\gamma_0 = 0$.

into account the effect of saturation due the population difference density reduction which obviously will be faster at lower pressure.

VI. GRADIENT

In this section we revisit our simulation results for wake amplification in 10 atm CO_2 mixture published in [14], with a set of parameters updated according to the above considerations and summarized in Table I. The e-beam radius is reduced to 30 μm (rms); resonance bandwidth, relative permittivity of the mixture and the resonance eigenmode are considered for pressure values of approximately 2 and 10 atm. As in the previous publication, the trigger beam is assumed to be density modulated at the resonant frequency of the medium—ω_0. The transverse density of the beam is assumed to be a Gaussian, $f_\perp(r) = (1/2\pi\sigma_b^2)\exp(-r^2/2\sigma_b^2)$, thus the current density is expressed by

$$J_z(r,\tau) = f_\perp(r)\mathrm{v}\frac{Q_{\mathrm{total}}}{L_{\mathrm{tr}}}[1 + A_{\mathrm{m}}\cos(\omega_0\tau)] \times \left[h(\tau) - h\left(\tau - \frac{L_{\mathrm{tr}}}{\mathrm{v}}\right)\right]. \quad (33)$$

The objective of numerical simulation is an exact evaluation of longitudinal electric field as defined by Eq. (4) for a trigger beam in the form defined by Eq. (33). The procedure employed is to find numerically roots of the denominator of the spectrum function, Eq. (5), for a specific mode s of interest. When the roots are known, the integral in Eq. (4) may be solved analytically and a contribution of each mode, including its propagating and evanescent components, to the wakefield is found exactly as a function of time and longitudinal coordinate for a given trigger bunch position z_σ. We had superimposed the calculation for the first 1000 modes of the wakefield. Radial

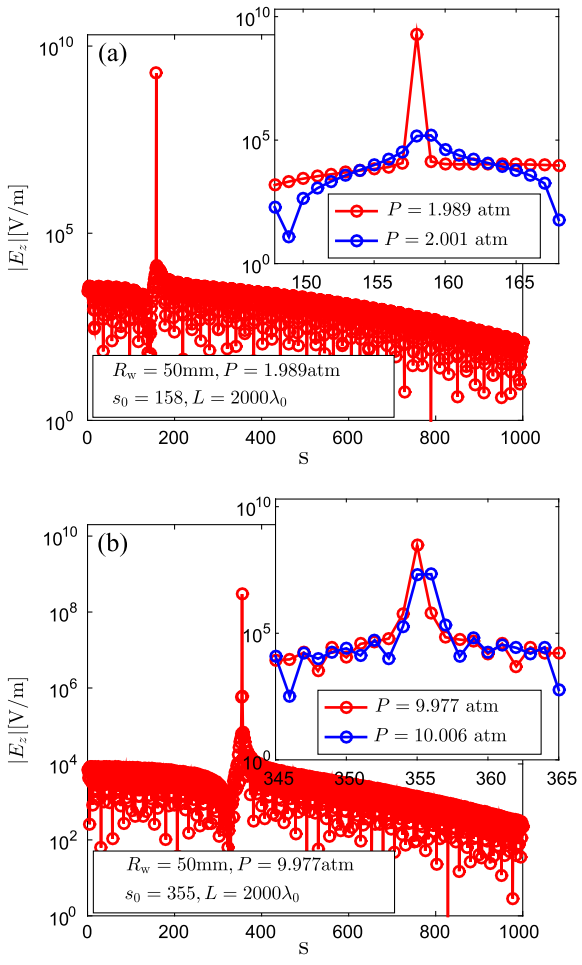

FIG. 7. Contribution of the various modes to E_z. In the inset we compare resonance and off-resonance conditions near the peak. (a) Pressure is approximately 2 atm; (b) pressure is approximately 10 atm.

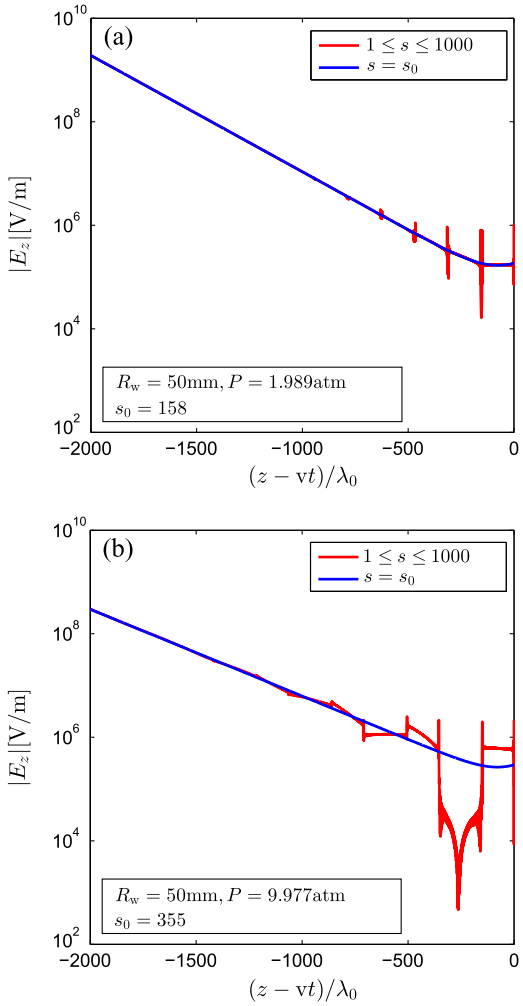

FIG. 8. Amplitude of E_z behind the trigger bunch (time domain) for 1000 Bessel harmonics (red curve), the single resonant Bessel harmonic (blue curve). For both (a) 2 atm and (b) 10 atm about 1000 λ_0 away from the trigger bunch the resonant mode is dominant.

distributions of the trigger and accelerated beams are taken to be of identical Gaussian form and assuming the beam transverse dimensions to be small relative to waveguide radius the radial component of the Green's function is averaged as $2\pi \int_0^\infty dr' f_\perp(r') r' J_0(p_s r'/R_w) \times 2\pi \int_0^\infty dr f_\perp(r) r J_0(p_s r/R_w) = \exp(-p_s^2 \sigma_b^2/R_w^2)$. All that is left is to integrate the result over any given trigger bunch distribution which may be done numerically for a desired resolution in z_σ. In the particular case of trigger bunch described by Eq. (33) the integration is done analytically with a result for propagating and evanescent components of each mode in a form of Eq. (14).

It is important to emphasize at this point that the results of numerical assessment presented here are exact only in the framework of the linear analysis of the model. Investigation of the nonlinear regime for a similar configuration is presented in Ref. [22].

Figure 7 shows the contribution of the various modes at a distance $L = 2000\lambda_0$ behind the modulated trigger bunch for the mixture pressure values of 2 and 10 atm. Due to reduced beam radius the contribution of the low eigenmodes is lower and the contribution of the modes in vicinity of the resonance is higher, comparing to the 4 mm beam considered in our simulations in [14]. As a result, according to the linear model, while no saturation or gas breakdown is taken in account, the amplified wake exceeds electric field values of the order of GV/m already at $2000\lambda_0$ (~2 cm) behind the trigger.

For both pressure values only one or two modes in the vicinity of the resonance have a significant contribution and the rest are orders of magnitude weaker. While waveguide radius is unchanged for both cases (50 mm) the mixture pressure is adjusted (a) to 1.989 atm, corresponding to the resonance mode $s_0 = 158$; and (b) to 9.977 atm, corresponding to the resonance mode $s_0 = 355$. The insets

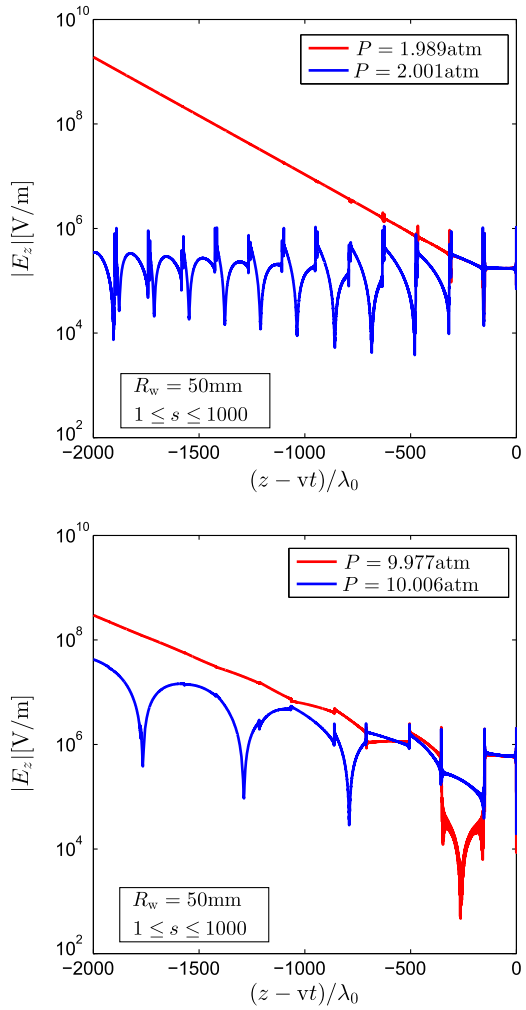

FIG. 9. Amplitude of E_z behind the trigger bunch (time domain) employing 1000 Bessel harmonics in the case of resonance $\omega_{s_0,C} = \omega_0$ (red curve) and off resonance (blue curve).

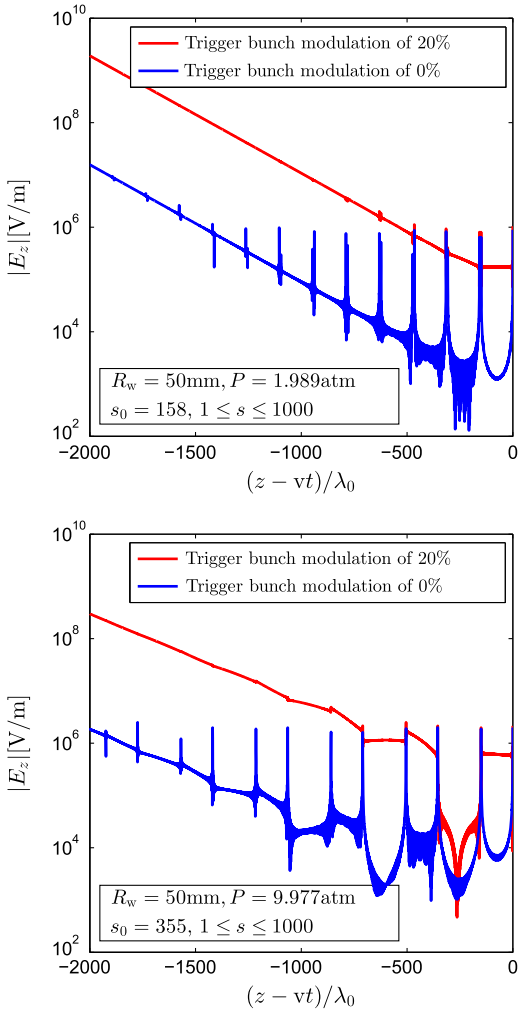

FIG. 10. Amplitude of E_z behind the trigger bunch (time domain) employing 1000 Bessel harmonics in the case of resonance $\omega_{s_0,C} = \omega_0$ with modulated (red curve) and not modulated (blue curve) beam. The typical signal to noise ratio is about 40 dB for an initial 20% modulation for both pressure values.

illustrate off-resonance behavior—the pressure is shifted in order to have the resonance exactly between two eigenfrequencies: (a) 2.001 atm sets the resonance between modes 158 and 159; (b) 10.006 atm sets the resonance between modes 355 and 356. It may be seen from Fig. 7 that the exact tuning of the eigenfrequency is more critical at lower pressure—the amplitude of the amplified wake is reduced by about 4 orders of magnitude while off resonance at pressure of 2 atm and only by about 1 order of magnitude at pressure of 10 atm. The amplification is higher at lower pressure due to the fact that the Cherenkov slippage factor is reduced with pressure. However one shall keep in mind that this result is true for the linear model and the picture will change dramatically when the energy depletion by the growing wake will be considered. In the latter case more dilute medium, storing less energy, will deplete faster eventually limiting the amplification.

The enhanced exponential gain is clearly revealed in Fig. 8 where the gradient is illustrated for two cases: a single resonance mode $(s = s_0)$ and first 1000 modes $(1 \le s \le 1000)$; the asymptotic behavior in both cases is determined by the resonant mode (s_0) while all the others determine the "near-field," adjacent to the trigger bunch.

Whether the resonance condition is exactly satisfied or only approximately, may make significant difference as revealed in Fig. 9. Finally, Fig. 10 shows that typically a signal to noise ratio of 40 dB may be expected in the case of a 20% modulated beam comparing to a zero-modulated beam regardless of the pressure—2 or 10 atm.

VII. REALISTIC CONFIGURATION

While the configuration of a uniformly filled metallic waveguide has its great advantage since it facilitates a relatively simple analytic set of expressions that describe the wake amplification, it has three deficiencies. (i) A relativistic beam may ionize the gas mixture and as a result, the active medium will be altered or even destroyed. (ii) For the parameters of interest, the overall pressure of the gas mixture must be of the order of 8–10 atm's whereas in the accelerator's tunnel, the pressure is many orders of magnitude lower. Two thin vacuum windows between the two regions would be exposed to a huge pressure difference. Elevating the thickness may reduce this problem but it generates a worst one: the emittance of the electron beam traversing the two windows will increase dramatically. (iii) Propagation of an e-beam in an 8–10 atm gas mixture is accompanied by emittance increase associated with small-angle scattering.

In order to avoid these impediments, we return now to the original configuration that we described in Fig. 2 whereby a vacuum tunnel is surrounded by a *thick dielectric layer* which in turn is surrounded the active gas mixture. Since we know that a Bragg structure that can confine the Cherenkov radiation in its inner part and allow propagating waves from the outside inwards, can be designed, we replace the Bragg wall with a metallic wall of infinite conductivity.

In Appendixes D and E we demonstrate that the trigger bunch, which moves in the vacuum region, generates Cherenkov radiation in all of the volume including the active medium. The latter amplifies the Cherenkov wake according to a similar amplification factor, up to a *filling factor*

$$F_{\mathrm{f}} = \frac{1}{1 + \frac{\varepsilon_g}{\varepsilon_{\mathrm{r}}} \frac{R_{\mathrm{ext}} - R_{\mathrm{int}}}{R_{\mathrm{w}} - R_{\mathrm{ext}}}} \tag{34}$$

namely,

$$\omega_{\pm} = \omega_0 + j\frac{\Delta\omega}{4}\left[1 \pm \sqrt{1 + 16a^2 F_{\mathrm{f}}}\right] \equiv \omega_0 + j\delta\omega_{\pm} \tag{35}$$

provided *two necessary conditions* are satisfied by the thick layer and the active medium

$$\begin{aligned} \frac{\omega_0}{c}\sqrt{\varepsilon_{\mathrm{r}} - 1}(R_{\mathrm{w}} - R_{\mathrm{ext}}) &= \frac{\pi}{2} + \pi n \gg 1, \\ \frac{\omega_0}{c}\sqrt{\varepsilon_{\mathrm{g}} - 1}(R_{\mathrm{ext}} - R_{\mathrm{int}}) &= \frac{\pi}{2} + \pi m \gg 1. \end{aligned} \tag{36}$$

The present configuration has three geometric parameters: R_{int} is the radius of the vacuum tunnel, R_{ext} is the external radius of the thick dielectric layer; as before, R_{w} is the radius of the waveguide. The conditions in Eq. (36) reduce the number of degrees of freedom to 1. The third constraint emerges from the condition that, given a uniformly filled waveguide of radius $R_{\mathrm{w}}^{(\mathrm{fill})}$, we require that the *energy stored* in the medium is the same in the glass-loaded structure as in the filled waveguide thus

$$\pi(R_{\mathrm{w}}^{(\mathrm{fill})})^2 = \pi R_{\mathrm{w}}^2 - \pi R_{\mathrm{ext}}^2. \tag{37}$$

Explicitly, the geometric parameters are given by

$$\begin{aligned} R_{\mathrm{ext}} &= R_{\mathrm{w}}^{(\mathrm{fill})}\frac{1}{2}\left(\frac{p_{s_0}}{\pi/2 + \pi n} - \frac{\pi/2 + \pi n}{p_{s_0}}\right) \\ R_{\mathrm{int}} &= R_{\mathrm{w}}^{(\mathrm{fill})}\left[\begin{array}{c} \frac{1}{2}\left(\frac{p_{s_0}}{\pi/2+\pi n} - \frac{\pi/2+\pi n}{p_{s_0}}\right) \\ -\frac{\sqrt{\varepsilon_{\mathrm{r}}-1}}{\sqrt{\varepsilon_{\mathrm{g}}-1}}\frac{\pi/2+\pi m}{p_{s_0}} \end{array}\right] \\ R_{\mathrm{w}} &= \frac{1}{2}R_{\mathrm{w}}^{(\mathrm{fill})}\left(\frac{p_{s_0}}{\pi/2 + \pi n} + \frac{\pi/2 + \pi n}{p_{s_0}}\right). \end{aligned} \tag{38}$$

A. Dynamics

As in the uniform case, our next step is to determine the dynamics of the wake. In Appendix E it is shown that the secondary electric field at its front $(\tau = 0)$ for a charged ring of radius r_σ is given by

$$E_z^{(\mathrm{sec})} = \frac{q}{2\pi\varepsilon_0\varepsilon_\mathrm{r}}\frac{1}{\sqrt{1+16F_\mathrm{f}a^2}} \times \frac{F_\mathrm{f}\varepsilon_\mathrm{g}/\sqrt{\varepsilon_\mathrm{g}-1}}{2\pi(R_\mathrm{w}-R_\mathrm{ext})/\lambda_0}\frac{I_0(\Gamma_0 r_\sigma)I_0(\Gamma_0 r)}{R_\mathrm{int}^2}, \quad (39)$$

where $\Gamma_0 \equiv 2\pi/\gamma\beta\lambda_0$, thus

$$E_z\left(\tau+\frac{z_\sigma}{c\beta}\right) = E_z^{(\mathrm{sec})}U^{(\mathrm{glass})}\left(\tau+\frac{z_\sigma}{c\beta}\right), \quad (40)$$

where

$$U^{(\mathrm{glass})}(\tau) \equiv \frac{h(\tau)}{\delta\omega_+ - \delta\omega_-} \times \left\{ \begin{array}{l} \frac{\delta\omega_-\delta\omega_+}{\omega_0}\sin(\omega_0\tau) \\ \times\left[\begin{array}{l}\exp(-\delta\omega_+\tau) \\ -\exp(-\delta\omega_-\tau)\end{array}\right] \\ +\cos(\omega_0\tau) \\ \times\left[\begin{array}{l}\delta\omega_+\exp(-\delta\omega_-\tau) \\ -\delta\omega_-\exp(-\delta\omega_+\tau)\end{array}\right] \end{array} \right\}$$

$$\delta\omega_\pm = \frac{\Delta\omega}{4}\left[1\pm\sqrt{1+16a^2F_\mathrm{f}}\right]. \quad (41)$$

As in the simplified model we calculate spontaneous and coherent power for the trigger bunch with Gaussian transverse and longitudinal distributions

$$P^{(\mathrm{spo,g})} = \frac{-N_\mathrm{el}q^2\mathrm{v}}{4\pi\varepsilon_0 R_\mathrm{int}^2}\frac{F_\mathrm{f}\frac{\varepsilon_\mathrm{g}}{\varepsilon_\mathrm{r}}\sqrt{\frac{1}{\varepsilon_\mathrm{g}-1}}}{\frac{\omega_0}{c}(R_\mathrm{w}-R_\mathrm{ext})}\frac{1}{\sqrt{1+16F_\mathrm{f}a^2}}F_\perp^{(\mathrm{spo,g})} \quad (42)$$

$$P^{(\mathrm{coh,g})} = \frac{-N_\mathrm{el}q^2\mathrm{v}}{4\pi\varepsilon_0 R_\mathrm{int}^2}\frac{F_\mathrm{f}\frac{\varepsilon_\mathrm{g}}{\varepsilon_\mathrm{r}}\sqrt{\frac{1}{\varepsilon_\mathrm{g}-1}}}{\frac{\omega_0}{c}(R_\mathrm{w}-R_\mathrm{ext})}\frac{1}{\sqrt{1+16F_\mathrm{f}a^2}} \times (N_\mathrm{el}-1)F_\perp^{(\mathrm{coh,g})}F_\parallel^{(\mathrm{coh,g})} \quad (43)$$

implying that the power generated by the particles is

$$P^{(\mathrm{tot,g})} = \frac{-N_\mathrm{el}q^2\mathrm{v}}{4\pi\varepsilon_0 R_\mathrm{int}^2}\frac{F_\mathrm{f}\frac{\varepsilon_\mathrm{g}}{\varepsilon_\mathrm{r}}\sqrt{\frac{1}{\varepsilon_\mathrm{g}-1}}}{\frac{\omega_0}{c}(R_\mathrm{w}-R_\mathrm{ext})}\frac{1}{\sqrt{1+16F_\mathrm{f}a^2}} \times [F_\perp^{(\mathrm{spo,g})} + (N_\mathrm{el}-1)F_\parallel^{(\mathrm{coh,g})}F_\perp^{(\mathrm{coh,g})}]. \quad (44)$$

Here $F_\perp^{(\mathrm{spo,g})} \equiv 2\pi\int_0^{R_\mathrm{int}} drrf_\perp(r)I_0^2(\Gamma_0 r_\sigma)$, $F_\perp^{(\mathrm{coh,g})} \equiv [2\pi\int_0^{R_\mathrm{int}} drrf_\perp(r)I_0(\Gamma_0 r)]^2$ and $F_\parallel^{(\mathrm{coh,g})} \equiv 2\int_{-\infty}^{\infty} dzf_\parallel(z)\times\int_{-\infty}^{\infty} d\zeta f_\parallel(\zeta)U^{(\mathrm{glass})}(\frac{z-\zeta}{c\beta})$.

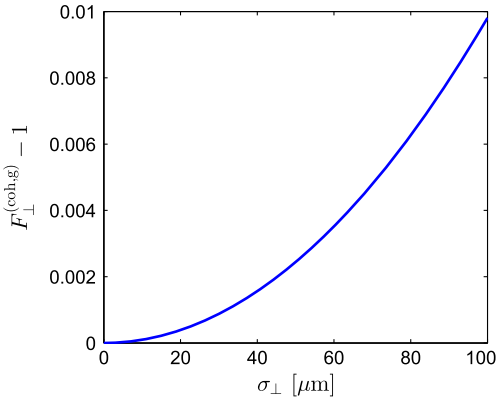

FIG. 11. Coherent $F_\perp^{(\mathrm{coh,g})}$ transverse form factors for a Gaussian transverse distribution as functions of the rms value $\sigma_\perp$ for $\gamma = 600$.

For $f_\perp(r) = (1/2\pi\sigma_\perp^2)\exp(-r^2/2\sigma_\perp^2)$ and assuming $R_\mathrm{int} \gg \sigma_\perp$, the transverse form factors may be evaluated analytically as a function of parameter $\bar{\sigma}_{\perp\mathrm{g}} \equiv (2\pi/\gamma\beta)\sigma_\perp/\lambda_0$:

$$F_\perp^{(\mathrm{spo,g})} \simeq \frac{1}{\sigma_\perp^2}\int_0^\infty drr\exp\left(-\frac{r^2}{2\sigma_\perp^2}\right)I_0^2(\Gamma_0 r_\sigma) = \exp(\bar{\sigma}_{\perp(\mathrm{g})}^2)I_0(\bar{\sigma}_{\perp(\mathrm{g})}^2) \quad (45)$$

$$F_\perp^{(\mathrm{coh,g})} \simeq \left[\frac{1}{\sigma_\perp^2}\int_0^\infty drr\exp\left(-\frac{r^2}{2\sigma_\perp^2}\right)I_0(\Gamma_0 r)\right]^2 = \exp(\bar{\sigma}_{\perp(\mathrm{g})}^2). \quad (46)$$

Solutions for integrals in Eqs. (45) and (46) may be found in [15], Eq. (10.43.28). Dependency of the coherent transverse form factor on the transverse distribution rms value is shown in Fig. 11. For our parameters the spontaneous transverse form factor differs negligibly from the coherent for the beam cross section of relevant scale.

For a typical set of parameters, which will be defined in the next section, the filling factor is close to unity and consequently the longitudinal form factor for realistic configuration is close to one for the simplified model presented in Fig. 4, namely $F_\parallel^{(\mathrm{coh,g})} \simeq F_\parallel^{(\mathrm{coh})}$.

VIII. DISCUSSION

In Ref. [10] we demonstrated that for a CO_2 mixture similar to that reported by the UCLA group, a gradient of the order of GV/m is feasible. This is limited by two different processes: saturation and ionization. With this regard, the CO_2 mixture is not necessarily the best medium, in fact, an ionized active medium (such as Ar^+) may prove to be a better choice simply because the second ionization occurs at much higher field intensity. But maximizing neither of the two is the scope of this analysis.

In Ref. [14] we analyzed the beam loading effect for the simplified model in the linear regime. It was shown that exponential gain may compensate for the wakefield generated by *accelerated* bunches and eliminate the effect. It is a matter of design to apply the same technique to the realistic configuration presented here. In the saturated regime there is a tradeoff between energetic efficiency of the acceleration process and the scale of beam loading effect. This case is addressed in Ref. [23].

The updated configuration considered in the present paper prevents collisions of the bunch electrons with the active medium components eliminating effects of scattering and collisional ionization. Still one shall be aware that field intensity of the amplified wake may cause ionization of medium; also we do not expect this to happen at field intensities below 2 GV/m [10]. Accurate assessment of the wakefield intensity threshold for ionization of a particular gas mixture is out of the scope of this paper.

Electrical breakdown of the confining structure material also shall be taken into account in a framework of realistic design. The amplified wakefield has its maximum at the vacuum-dielectric interface, where both longitudinal and radial components are contributing to the total field value and the ratio between field component amplitudes in the vacuum channel is

$$\frac{|E_r|}{|E_z|} \simeq \frac{\omega_0/\mathrm{v}}{2\pi/\gamma\beta\lambda_0} = \gamma. \tag{47}$$

Thus the total electric field amplitude on the interface is related to the longitudinal field amplitude on the vacuum channel axis as

$$|E_{\mathrm{tot}}(r = R_{\mathrm{int}})| = |E_z(r = 0)|\sqrt{I_0^2(\rho) + \gamma^2 I_1^2(\rho)}, \tag{48}$$

where $\rho \equiv 2\pi R_{\mathrm{int}}/\gamma\beta\lambda_0$. Equation (48) reveals that in order for the total electric field on the interface to be of the order of the longitudinal field on the axis of the vacuum channel, the radius of the latter shall be on the scale of the resonant wavelength. Assuming the length of an accelerated train of microbunches to be on the scale of $100\lambda_0$ the minimal duration τ_p of the amplified wake required in the CO_2 case is of an order of 3 ps. It is shown in Ref. [7] based on experimental data from Ref. [24] that for pulses on such a scale dielectric breakdown will limit the field by

$$E_{\mathrm{max}} = \sqrt{25.1/(0.5\varepsilon_0\varepsilon\mathrm{v}\tau_p^{3/4})} \times 10^3 \simeq 2\ \mathrm{GV/m}. \tag{49}$$

In this publication we presented the growth of the wake in a realistic configuration (glass loaded structure) in terms of a filling factor. In order to maintain a realistic gain, the filling factor needs to be of the order of 0.96. For example a typical set of parameters that ensure this value is specified next: $\varepsilon_g/\varepsilon_r \sim 2$, $R_w \simeq 50$ mm, $R_{\mathrm{ext}} \simeq 1.0$ mm, $R_{\mathrm{int}} \simeq 10\ \mu$m and length of interaction $d \simeq 2000\lambda_0$. The gain in this case may be defined as

$$G^{(\mathrm{glass})} \simeq 10\log\left\{\begin{array}{l}\sqrt{\frac{1}{1+16a^2F_{\mathrm{f}}}} \\ \times\exp[\frac{\Delta\omega}{4c\beta}d(\sqrt{1+16a^2F_{\mathrm{f}}}-1)]\end{array}\right\} \tag{50}$$

and for a filling factor of 0.96 the calculated gain is $G^{(\mathrm{glass})} = 28$ dB, about 1 dB less than the case $F_{\mathrm{f}} = 1.0$ namely $G^{(\mathrm{glass})} = 28.9$ dB.

Length of a typical bunch is expected to be on the scale of a hundred of resonant wavelengths and in the absence of amplification, in a *passive medium*, such a bunch will trigger no wake. We had shown that with a nonzero amplification, in an *active medium*, long bunches will trigger a wake even while not modulated. However trigger bunch modulation at the medium resonant frequency increases initial wake amplitude by a factor of $A_m\omega_0/2|\delta\omega_-|$, corresponding in our case to about 2 orders of magnitude for 20% density modulation.

For chosen active medium composition and structure geometry it is essentially convenient to tune the system to resonance regulating the gas mixture pressure. For a typical configuration at pressure of about 10 atm, separation between two adjacent pressure levels bringing the system to a resonance is about 5 kPa. Therefore pressure shall be tuned with accuracy on a level of tens Pa. Lowering the pressure will bring the system closer to Cherenkov threshold and thus make the wake growth larger (increased gain enhancement). However, system sensitivity to resonance tuning and trigger bunch energy spread will increase and even more importantly, assuming the relative population difference density unchanged, reduction of the pressure will reduce the saturation level of the wakefield.

ACKNOWLEDGMENTS

This study was supported by the Bi-National United States–Israel Science Foundation and Israel Science Foundation. We have benefited from valuable comments from Professor Chandrashekhar Joshi, University of California, Los Angeles, and Professor Patric Muggli, University of Southern California. M. Voin wishes to acknowledge fruitful discussions with Z. Toroker, Technion–Israel Institute of Technology.

APPENDIX A: ANALITICAL ESTIMATION OF THE LONGITUDINAL FORM FACTOR

For an analytical estimation of the longitudinal form factor $F_{\parallel}^{(\mathrm{coh})}$ we neglect the component of $U(\tau)$ proportional to $\sin(\omega_0\tau)$ in Eq. (7) and with definition $\omega_{\pm} \equiv \omega_0 + j\delta\omega_{\pm}$ rewrite the latter as

$$U(\tau) \simeq \frac{h(\tau)}{\delta\omega_+ - \delta\omega_-}\mathrm{Re}\begin{bmatrix}\delta\omega_+ \exp(j\omega_-\tau) \\ -\delta\omega_- \exp(j\omega_+\tau)\end{bmatrix}. \quad \text{(A1)}$$

For the sake of simplicity we approximate the Gaussian distribution by a shifted-up-cosine function $f_{\parallel\cos}(\zeta) = (\mathrm{K}/2\pi)[1+\cos(\mathrm{K}\zeta)]$, which is characterized by rms value $\sigma_\parallel$ when $\mathrm{K} = \sqrt{\pi^2/3-2}/\sigma_\parallel \equiv b/\sigma_\parallel$. Then, defining $k_\pm \equiv \omega_\pm/c \equiv k_0 + j\delta k_\pm$, the coherent transverse form factor may be found as

$$\begin{aligned} F^{(\mathrm{coh})}_{\parallel\cos} \simeq{}& \frac{(\mathrm{K}/2\pi)^2}{\delta\omega_+ - \delta\omega_-}\int_{-\pi/\mathrm{K}}^{\pi/\mathrm{K}} dz[1+\cos(\mathrm{K}z)] \\ &\times \int_{-\pi/\mathrm{K}}^{z} d\zeta[1+\cos(\mathrm{K}\zeta)] \\ &\times \left\{\begin{array}{l}\delta\omega_+ \exp[jk_-(z-\zeta)] \\ +\delta\omega_+ \exp[-jk_-(z-\zeta)] \\ -\delta\omega_- \exp[jk_+(z-\zeta)] \\ -\delta\omega_- \exp[-jk_+(z-\zeta)]\end{array}\right\}. \end{aligned} \quad \text{(A2)}$$

Solving the integrals we find

$$\begin{aligned} F^{(\mathrm{coh})}_{\parallel\cos} \simeq{}& \frac{\delta\omega_+}{\delta\omega_+ - \delta\omega_-}\left[\frac{\mathrm{K}^2}{\mathrm{K}^2 - k_-^2}\mathrm{sinc}\left(\pi\frac{k_-}{\mathrm{K}}\right)\right]^2 \\ &- \frac{\delta\omega_-}{\delta\omega_+ - \delta\omega_-}\left[\frac{\mathrm{K}^2}{\mathrm{K}^2 - k_+^2}\mathrm{sinc}\left(\pi\frac{k_+}{\mathrm{K}}\right)\right]^2. \end{aligned} \quad \text{(A3)}$$

Assuming $|\delta k_\pm| \ll k_0, \mathrm{K}$ we may further approximate Eq. (A3) and substituting the expressions for K and $k_\pm$ we finally have

$$\begin{aligned} F^{(\mathrm{coh})}_{\parallel\cos} \simeq{}& \left(\frac{b^2c^2}{b^2c^2 - \sigma_\parallel^2\omega_0^2}\right)^2 \mathrm{sinc}^2\left(\frac{\pi}{bc}\sigma_\parallel\omega_0\right) \\ &\times \frac{[\delta\omega_+\cosh^2(\frac{\pi}{bc}\sigma_\parallel\delta\omega_-) - \delta\omega_-\cosh^2(\frac{\pi}{bc}\sigma_\parallel\delta\omega_+)]}{\delta\omega_+ - \delta\omega_-}. \end{aligned} \quad \text{(A4)}$$

Parameter b here is defined as $b \equiv \sqrt{\pi^2/3-2} \simeq 1.14$. The function represented by Eq. (A4) for the resonant mode at our parameters is shown in Fig. 12.

Comparing the graph in Fig. 12 with the result of numeric calculation for Gaussian beam distribution shown in Fig. 4 we note that while qualitatively two functions looks similar, quantitatively they are significantly different. For instance, the first null in the longitudinal form factor for Gaussian distribution appears at $\sigma_\parallel \simeq 6.1$ μm, while for shifted-up-cosine distribution at $\sigma_\parallel \simeq 3.8$ μm; at the same time the form factor for shifted-up-cosine distribution has the first lobe about 3 orders of magnitude higher than the one for the Gaussian distribution. Evidently, the coherent longitudinal form factor is sensitive to the form of the trigger microbunch longitudinal distribution.

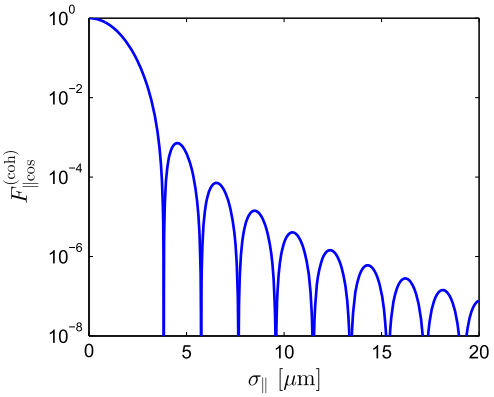

FIG. 12. Coherent longitudinal form factor $F^{(\mathrm{coh})}_{\parallel\cos}$ for a shifted-up-cosine longitudinal distribution as a function of the rms value $\sigma_\parallel$ for 10 atm active medium values summarized in Table I.

APPENDIX B: SOLUTION FOR DENSITY MODULATED TRIGGER BEAM

From Eq. (8) the field corespondent to a zero length bunch for large values of τ is approximated as

$$E_z^{(s_0,\sigma)}(\tau) = E_z^{(s_0,\sigma)}(0)\frac{\delta\omega_+}{\delta\omega_+ - \delta\omega_-}\mathrm{Re}[\exp(j\omega_-\tau)]. \quad \text{(B1)}$$

Looking for a solution for a density modulated triggering beam of length $L_\mathrm{t} = N_\lambda\lambda_0$ (where N_λ is a natural number) and a modulation index $0 \le A_m \le 1$ we consider the following:

$$\begin{aligned} E_z^{(s_0)} &\equiv E_z^{(s_0)}(\tau, L_\mathrm{t}, A_m) \\ &= \frac{1}{L_\mathrm{t}}\int_0^{L_\mathrm{t}} du\left[1 + A_m\cos\left(\frac{2\pi}{\lambda_0}u\right)\right]E_z^{(s_0,\sigma)}\left(\tau - \frac{u}{\mathrm{v}}\right). \end{aligned} \quad \text{(B2)}$$

Evaluating the integral we have

$$\begin{aligned} E_z^{(s_0)} ={}& E_z^{(s_0,\sigma)}(0)\frac{\delta\omega_+}{\delta\omega_+ - \delta\omega_-} \\ &\times \mathrm{Re}\left\{\begin{array}{l}\frac{\mathrm{v}}{j\omega_-}\exp(j\omega_-\tau)\frac{1-\exp(-\frac{j\omega_-}{\mathrm{v}}L_\mathrm{t})}{L_\mathrm{t}} \\ \times\left[1 + \frac{A_m}{1+(\frac{2\pi}{\lambda_0}\frac{\mathrm{v}}{j\omega_-})^2}\right]\end{array}\right\}. \end{aligned} \quad \text{(B3)}$$

A homogeneous bunch of a length equal to a round number of the resonance wavelengths of the medium, propagating in a medium with no spatial growth, namely a *passive medium*, triggers no wake. Observing the result in Eq. (B3) we note that even for a zero modulation of the triggering beam density the resulting wake is not zero as

long as $\delta\omega_\nu$ is not zero, meaning that in an *active medium* a nonmodulated bunch exceeding the resonance wavelength by many times will trigger a wake.

Substituting $\omega_\pm = \omega_0 + j\delta\omega_\pm$, $\delta\omega_\pm \equiv (\Delta\omega/4)(1\pm\sqrt{1+16a^2})$, and bearing in mind that $v \simeq c$, the amplitude of the field is approximated as

$$|E_z^{(s_0)}| \simeq E_z^{(s_0,\sigma)}(0)\frac{1+(1+16a^2)^{-1/2}}{2} \times \frac{1-\exp(-2\pi N_\lambda \frac{|\delta\omega_-|}{\omega_0})}{2\pi N_\lambda} \times \exp(-\delta\omega_-\tau)\begin{cases} 1 & A_m = 0 \\ \frac{A_m}{2}\frac{\omega_0}{|\delta\omega_-|} & A_m \sim 0.1. \end{cases} \quad \text{(B4)}$$

APPENDIX C: RELATIVE POPULATION DIFFERENCE CONSIDERATION

According to Siegman [20], Chapter 6.1, for a four-level laser system the pumping rate equation is written using optical approximation, which is appropriate at frequencies satisfying $\hbar\omega/k_BT \gg 1$. At this condition thermally stimulated relaxation rates are negligible comparing to spontaneous emission rates and the rate equations are written as

$$\frac{dN_4}{dt} = W_p(N_1 - N_4) - (\gamma_{43}+\gamma_{42}+\gamma_{41})N_4 \equiv W_p(N_1 - N_4) - N_4/\tau_4 \quad \text{(C1)}$$

$$\frac{dN_3}{dt} = \gamma_{43}N_4 - (\gamma_{32}+\gamma_{31})N_3 \equiv N_4/\tau_{43} - N_3/\tau_3 \quad \text{(C2)}$$

$$\frac{dN_2}{dt} = \gamma_{42}N_4 + \gamma_{32}N_3 - \gamma_{21}N_2 \equiv N_4/\tau_{42} + N_3/\tau_{32} - N_2/\tau_{21}. \quad \text{(C3)}$$

At steady state we have

$$N_4 = \frac{W_p\tau_4}{1+W_p\tau_4}N_1 \quad \text{(C4)}$$

$$N_3 = \frac{\tau_3}{\tau_{43}}N_4 \quad \text{(C5)}$$

$$N_2 = \left(\frac{\tau_{21}}{\tau_{32}} + \frac{\tau_{43}\tau_{21}}{\tau_{42}\tau_3}\right)N_3 \equiv \beta N_3. \quad \text{(C6)}$$

Here N_i are populations of correspondent levels, W_p is a pumping rate associated with pumping transition probability and γ_{ij} are the total decay rates, including both radiative and nonradiative, between correspondent levels and $\tau_{ij} \equiv 1/\gamma_{ij}$ are correspondent lifetimes.

Using conservation of atoms $N_1 + N_2 + N_3 + N_4 = N$ we may find the normalized population difference

$$\frac{N_3 - N_2}{N} = \frac{(1-\beta)\frac{\tau_3\tau_4}{\tau_{43}}W_p}{1+(1+\beta+2\frac{\tau_{43}}{\tau_3})\frac{\tau_3\tau_4}{\tau_{43}}W_p}. \quad \text{(C7)}$$

Let us take a closer look to the lifetime $\tau_3 \equiv 1/\gamma_3$. The total decay rate γ_3 is a sum of radiative and nonradiative decay rates. The latter shall be directly proportional to the atoms' density, Siegman [20], page 200:

$$\gamma_3 \equiv \gamma_{32\text{rad}} + \gamma_{32\text{nr}} + \gamma_{31\text{rad}} + \gamma_{31\text{nr}}. \quad \text{(C8)}$$

For simplicity of notation the decay rate on the lasing transition is denoted simply as $\gamma_{\text{rad}} \equiv \gamma_{32\text{rad}}$. Siegman defines a *fluorescence quantum efficiency* factor η [20], Eq. (6.10), as

$$\eta \equiv \frac{\gamma_{43}}{\gamma_4}\times\frac{\gamma_{\text{rad}}}{\gamma_3} = \frac{\tau_4}{\tau_{43}}\times\frac{\tau_3}{\tau_{\text{rad}}}. \quad \text{(C9)}$$

The first ratio in Eq. (C9) indicates what fraction of atoms decaying from level 4 decays to level 3 and not to other levels. The second ratio indicates what fraction of decay from level 3 is the radiative decay into level 2. Obviously for a good laser system the factor η shall be close to unity, Siegman [20], Equation (6.12).

In summary the following assumptions are appropriate: (i) level 4 decays primarily into level 3, namely $\tau_4 \approx \tau_{43}$ and consequently $\tau_{43} \ll \tau_{42}$; (ii) decay rate of level 4 into level 3 is much faster than level 3 into level 2 and directly into level 1, namely $\tau_{43} \ll \tau_3$; (iii) decay rate of level 2 into level 1 is much faster than level 3 into level 2 and directly into level 1, namely $\tau_{21} \ll \tau_3 = \tau_{32} + \tau_{31}$. Thus $\tau_4/\tau_{43} \approx 1$, $\beta \ll 1$, $\tau_{43}/\tau_3 \ll 1$ and Eq. (C7) may be approximated using the definition (C9) as

$$\frac{\Delta n}{n_0} = \frac{N_3 - N_2}{N} \approx \frac{\eta W_p\tau_{\text{rad}}}{1+\eta W_p\tau_{\text{rad}}} \approx \frac{W_p\tau_{\text{rad}}}{1+W_p\tau_{\text{rad}}}. \quad \text{(C10)}$$

The last expression holds while the system may be considered as a "good laser system" according to Siegman's terminology, namely $\beta \ll 1$ and $\eta \approx 1$. We assume that for the pressure range up to 10 atm in the CO_2 laser mixture, similar to that described in UCLA [18], these conditions are satisfied.

APPENDIX D: HOMOGENEOUS SOLUTION FOR REALISTIC CONFIGURATION

As a first step, we consider the electromagnetic problem in the *absence* of the electrons. A TM_{0s} mode is assumed to propagate along the waveguide and it is described by the z component of the magnetic vector potential, which reads

$$A_z \equiv A_z(r,z,\omega) = \exp(-jkz) \times \begin{cases} AI_0(\Gamma r) & 0 < r < R_{\rm int} \\ BJ_0(\kappa r) + CY_0(\kappa r) & R_{\rm int} < r < R_{\rm ext} \\ DT_0(\Lambda r) & R_{\rm ext} < r < R_{\rm w} \end{cases} \quad \text{(D1)}$$

wherein

$$\Gamma^2 = k^2 - \frac{\omega^2}{c^2} = \frac{\omega^2}{\mathrm{v}^2} - \frac{\omega^2}{c^2} = \frac{\omega^2}{c^2}\frac{1}{\beta^2\gamma^2}$$
$$\kappa^2 = \varepsilon_{\rm g}\frac{\omega^2}{c^2} - k^2 = \varepsilon_{\rm g}\frac{\omega^2}{c^2} - \frac{\omega^2}{\mathrm{v}^2} = \frac{\omega^2}{c^2}(\varepsilon_{\rm g} - \beta^{-2})$$
$$\Lambda^2 = \varepsilon_a\frac{\omega^2}{c^2} - k^2 = \varepsilon_a\frac{\omega^2}{c^2} - \frac{\omega^2}{\mathrm{v}^2} = \frac{\omega^2}{c^2}(\varepsilon_{\rm a} - \beta^{-2}) \quad \text{(D2)}$$

and

$$T_0(\Lambda r) \equiv J_0(\Lambda r)Y_0(\Lambda R_{\rm w}) - Y_0(\Lambda r)J_0(\Lambda R_{\rm w})$$
$$T_1(\Lambda r) \equiv J_1(\Lambda r)Y_0(\Lambda R_{\rm w}) - Y_1(\Lambda r)J_0(\Lambda R_{\rm w}). \quad \text{(D3)}$$

Boundary conditions at the vacuum-dielectric discontinuity ($r = R_{\rm int}$) imply

$$E_z:\ \frac{c^2}{j\omega}\left[\frac{\omega^2}{c^2} - \frac{\omega^2}{\mathrm{v}^2}\right]AI_0(\Gamma R_{\rm int}) = \frac{c^2}{j\omega\varepsilon_{\rm g}}\left[\varepsilon_{\rm g}\frac{\omega^2}{c^2} - \frac{\omega^2}{\mathrm{v}^2}\right][BJ_0(\kappa R_{\rm int}) + CY_0(\kappa R_{\rm int})]$$
$$H_\phi:\ \Gamma AI_1(\Gamma R_{\rm int}) = -\kappa[BJ_1(\kappa R_{\rm int}) + CY_1(\kappa R_{\rm int})] \quad \text{(D4)}$$

whereas the second discontinuity of the thick-dielectric layer ($r = R_{\rm ext}$) provides

$$E_z:\ \frac{c^2}{j\omega\varepsilon_{\rm g}}\left[\varepsilon_{\rm g}\frac{\omega^2}{c^2} - \frac{\omega^2}{\mathrm{v}^2}\right][BJ_0(\kappa R_{\rm ext}) + CY_0(\kappa R_{\rm ext})] = \frac{c^2}{j\omega\varepsilon_a}\left[\varepsilon_a\frac{\omega^2}{c^2} - \frac{\omega^2}{\mathrm{v}^2}\right]DT_0(\Lambda R_{\rm ext}),$$
$$H_\phi:\ -\kappa[BJ_1(\kappa R_{\rm ext}) + CY_1(\kappa R_{\rm ext})] = -\Lambda T_1(\Lambda R_{\rm ext}). \quad \text{(D5)}$$

Defining

$$g_{\rm int} = \sqrt{\varepsilon_g - 1}\frac{\omega}{c}R_{\rm int}, \qquad g_{\rm ext} = \sqrt{\varepsilon_g - 1}\frac{\omega}{c}R_{\rm ext},$$
$$a_{\rm ext} = \sqrt{\varepsilon_a - 1}\frac{\omega}{c}R_{\rm ext}, \qquad a_{\rm w} = \sqrt{\varepsilon_a - 1}\frac{\omega}{c}R_{\rm w},$$
$$u_{\rm int} = \frac{2\varepsilon_g}{\sqrt{\varepsilon_g - 1}\frac{\omega}{c}R_{\rm int}} \quad \text{(D6)}$$

and assuming $\gamma \to \infty$ the dispersion relation may be deduced from

$$u_{\rm int} = \frac{BJ_0(g_{\rm int}) + CY_0(g_{\rm int})}{BJ_1(g_{\rm int}) + CY_1(g_{\rm int})}$$
$$\frac{\varepsilon_g\sqrt{\varepsilon_a - 1}}{\varepsilon_a\sqrt{\varepsilon_g - 1}}\frac{T_0(a_{\rm ext})}{T_1(a_{\rm ext})} = \frac{BJ_0(g_{\rm ext}) + CY_0(g_{\rm ext})}{BJ_1(g_{\rm ext}) + CY_1(g_{\rm ext})}. \quad \text{(D7)}$$

Since in practice $u_{\rm int} \ll 1$ we conclude that $BJ_0(g_{\rm int}) + CY_0(g_{\rm int}) \simeq 0$ implying

$$\frac{\varepsilon_g\sqrt{\varepsilon_a - 1}}{\varepsilon_a\sqrt{\varepsilon_g - 1}}\frac{J_0(a_{\rm ext})Y_0(a_{\rm w}) - Y_0(a_{\rm ext})J_0(a_{\rm w})}{J_1(a_{\rm ext})Y_0(a_{\rm w}) - Y_1(a_{\rm ext})J_0(a_{\rm w})} = \frac{Y_0(g_{\rm ext})J_0(g_{\rm int}) - Y_0(g_{\rm int})J_0(g_{\rm ext})}{Y_1(g_{\rm ext})J_0(g_{\rm int}) - Y_0(g_{\rm int})J_1(g_{\rm ext})}. \quad \text{(D8)}$$

For large arguments $g_{\rm int}$, $g_{\rm ext}$, $a_{\rm w}$, $a_{\rm ext} \gg 1$:

$$\frac{\varepsilon_g\sqrt{\varepsilon_a - 1}}{\varepsilon_a\sqrt{\varepsilon_g - 1}}\tan\left[\frac{\omega}{c}\sqrt{\varepsilon_a - 1}(R_{\rm w} - R_{\rm ext})\right] = -\tan\left[\frac{\omega}{c}\sqrt{\varepsilon_{\rm g} - 1}(R_{\rm ext} - R_{\rm int})\right]. \quad \text{(D9)}$$

Option I.—At resonance $\omega = \omega_0$ we design the glass layer such that

$$\tan\left[\frac{\omega_0}{c}\sqrt{\varepsilon_{\rm r} - 1}(R_{\rm w} - R_{\rm ext})\right] = 0 \Rightarrow \frac{\omega_0}{c}\sqrt{\varepsilon_{\rm r} - 1}(R_{\rm w} - R_{\rm ext}) = \pi n \gg 1$$
$$\tan\left[\frac{\omega_0}{c}\sqrt{\varepsilon_{\rm g} - 1}(R_{\rm ext} - R_{\rm int})\right] = 0 \Rightarrow \frac{\omega_0}{c}\sqrt{\varepsilon_{\rm g} - 1}(R_{\rm ext} - R_{\rm int}) = \pi m \gg 1. \quad \text{(D10)}$$

Thus assuming $\omega = \omega_0 + \delta\omega$ and $\varepsilon_{\rm a} = \varepsilon_{\rm r} + \delta\varepsilon$,

$$\frac{\varepsilon_g\sqrt{\varepsilon_{\rm r} - 1}}{\varepsilon_{\rm r}\sqrt{\varepsilon_g - 1}}\left[\begin{matrix}\frac{\delta\omega}{c}\sqrt{\varepsilon_{\rm r} - 1}(R_{\rm w} - R_{\rm ext}) \\ +\frac{\omega_0}{c}\frac{1}{2\sqrt{\varepsilon_{\rm r} - 1}}\delta\varepsilon(R_{\rm w} - R_{\rm ext})\end{matrix}\right] = -\left[\frac{\delta\omega}{c}\sqrt{\varepsilon_{\rm g} - 1}(R_{\rm ext} - R_{\rm int})\right], \quad \text{(D11)}$$

hence

$$\delta\omega = -\frac{\omega_0}{2}\frac{1}{(\varepsilon_{\rm r} - 1) + (\varepsilon_{\rm g} - 1)\frac{\varepsilon_{\rm r}}{\varepsilon_g}\frac{R_{\rm ext} - R_{\rm int}}{R_{\rm w} - R_{\rm ext}}}\delta\varepsilon. \quad \text{(D12)}$$

At the limit $\bar{\varepsilon} \to 0$ the dispersion relation is independent of $\bar{\varepsilon}$ therefore irrelevant to our needs.

Option II.—The dispersion relation may be rewritten as

$$\frac{\varepsilon_g\sqrt{\varepsilon_a-1}}{\varepsilon_a\sqrt{\varepsilon_g-1}}\cot\left[\frac{\omega}{c}\sqrt{\varepsilon_{\rm g}-1}(R_{\rm ext}-R_{\rm int})\right] = -\cot\left[\frac{\omega}{c}\sqrt{\varepsilon_a-1}(R_{\rm w}-R_{\rm ext})\right]. \tag{D13}$$

At resonance $\omega=\omega_0$,

$$\begin{aligned}&\cot\left[\frac{\omega_0}{c}\sqrt{\varepsilon_{\rm r}-1}(R_{\rm w}-R_{\rm ext})\right]=0\\ &\Rightarrow \frac{\omega_0}{c}\sqrt{\varepsilon_{\rm r}-1}(R_{\rm w}-R_{\rm ext})=\frac{\pi}{2}+\pi n\gg 1\\ &\cot\left[\frac{\omega_0}{c}\sqrt{\varepsilon_{\rm g}-1}(R_{\rm ext}-R_{\rm int})\right]=0\\ &\Rightarrow \frac{\omega_0}{c}\sqrt{\varepsilon_{\rm g}-1}(R_{\rm ext}-R_{\rm int})=\frac{\pi}{2}+\pi m\gg 1\end{aligned} \tag{D14}$$

thus

$$\delta\omega=-\frac{\omega_0}{2}\frac{1}{1+\frac{\varepsilon_{\rm g}}{\varepsilon_{\rm r}}\frac{R_{\rm ext}-R_{\rm int}}{R_{\rm w}-R_{\rm ext}}}\frac{\delta\varepsilon}{\varepsilon_{\rm r}-1}. \tag{D15}$$

Further, up to the filling factor $F_{\rm f}=[1+\varepsilon_g(R_{\rm ext}-R_{\rm int})/\varepsilon_{\rm r}(R_{\rm w}-R_{\rm ext})]^{-1}$ the expression is identical to the fully filled waveguide

$$\delta\omega=-\frac{\omega_0}{2}\frac{\delta\varepsilon}{\varepsilon_{\rm r}-1} \tag{D16}$$

and the eigenfrequencies $\omega_\pm\equiv\omega_0+j\delta\omega_\pm=\omega_0+(j\Delta\omega/4)[1\pm\sqrt{1+16a^2F_{\rm f}}]$.

APPENDIX E: NONHOMOGENEOUS SOLUTION FOR REALISTIC CONFIGURATION

The nonhomogeneous solution namely, in the presence of a charged ring of radius r_σ is found as

$$\begin{aligned}&A_{z,r_\sigma}(r,z,\omega)\\ &\quad=\exp(-jkz)\\ &\quad\times\begin{cases}AI_0(\Gamma r)+A_p\frac{K_0(\Gamma r_\sigma)}{I_0(\Gamma r_\sigma)}I_0(\Gamma r) & 0<r<r_\sigma\\ AI_0(\Gamma r)+A_pK_0(\Gamma r) & r_\sigma<r<R_{\rm int}\\ BJ_0(\kappa r)+CY_0(\kappa r) & R_{\rm int}<r<R_{\rm ext}\\ DT_0(\Lambda r) & R_{\rm ext}<r<R_{\rm w},\end{cases}\end{aligned} \tag{E1}$$

wherein Γ, κ, Λ, T_0 and T_1 are defined by Eq. (D2), and A_p is assumed to be known $A_p=-[\mu_0 q/(2\pi)^2]I_0(\omega r_\sigma/\gamma\beta c)$. As in Appendix D the boundary conditions at $r=R_{\rm int}$ imply a set of equations similar to Eq. (D4) with the addition of terms proportional to A_p:

$$\begin{aligned}&E_z:\ \frac{c^2}{j\omega}\left[\frac{\omega^2}{c^2}-\frac{\omega^2}{{\rm v}^2}\right][AI_0(\Gamma R_{\rm int})+A_pK_0(\Gamma R_{\rm int})]\\ &\quad=\frac{c^2}{j\omega\varepsilon_{\rm g}}\left[\varepsilon_{\rm g}\frac{\omega^2}{c^2}-\frac{\omega^2}{{\rm v}^2}\right][BJ_0(\kappa R_{\rm int})+CY_0(\kappa R_{\rm int})]\\ &H_\phi:\ \Gamma[AI_1(\Gamma R_{\rm int})-A_pK_1(\Gamma R_{\rm int})]\\ &\quad=-\kappa[BJ_1(\kappa R_{\rm int})+CY_1(\kappa R_{\rm int})].\end{aligned} \tag{E2}$$

The boundary condition at $r=R_{\rm ext}$ provides a set of equations identical to Eq. (D5).

Using definitions in Eq. (D6) and defining

$$b=\frac{\omega}{\gamma\beta c}R_{\rm int} \tag{E3}$$

the amplitude in vacuum is

$$A=-\frac{K_0(b)+\zeta_{\rm int}K_1(b)}{I_0(b)-\zeta_{\rm int}I_1(b)}A_p \tag{E4}$$

wherein

$$\begin{aligned}\zeta_{\rm ext}&\equiv\frac{\varepsilon_{\rm g}}{\varepsilon_a}\frac{a_{\rm ext}}{g_{\rm ext}}\frac{T_0(a_{\rm ext})}{T_1(a_{\rm ext})}\\ \zeta_{\rm int}&\equiv\frac{1}{\varepsilon_{\rm g}}\frac{g_{\rm int}}{b}\frac{-\frac{Y_0(g_{\rm ext})-\zeta_{\rm ext}Y_1(g_{\rm ext})}{J_0(g_{\rm ext})-\zeta_{\rm ext}J_1(g_{\rm ext})}J_0(g_{\rm int})+Y_0(g_{\rm int})}{-\frac{Y_0(g_{\rm ext})-\zeta_{\rm ext}Y_1(g_{\rm ext})}{J_0(g_{\rm ext})-\zeta_{\rm ext}J_1(g_{\rm ext})}J_1(g_{\rm int})+Y_1(g_{\rm int})}.\end{aligned} \tag{E5}$$

For large arguments, $g_{\rm int},g_{\rm ext}\gg 1$ and $b\to 0$

$$\begin{aligned}\zeta_{\rm ext}&\simeq\frac{\varepsilon_{\rm g}}{\varepsilon_a}\frac{a_{\rm ext}}{g_{\rm ext}}\tan(a_{\rm w}-a_{\rm ext})\equiv\bar\zeta_{\rm ext}\tan(a_{\rm w}-a_{\rm ext})\\ \zeta_{\rm int}&\simeq\frac{1}{\varepsilon_{\rm g}}\frac{g_{\rm int}}{b}\frac{1+\zeta_{\rm ext}\cot(g_{\rm ext}-g_{\rm int})}{\cot(g_{\rm ext}-g_{\rm int})+\zeta_{\rm ext}}\end{aligned} \tag{E6}$$

$$\begin{aligned}A&=-\frac{A_p\frac{1+\bar\zeta_{\rm ext}\tan(a_{\rm w}-a_{\rm ext})\cot(g_{\rm ext}-g_{\rm int})}{\cot(g_{\rm ext}-g_{\rm int})+\zeta_{\rm ext}\tan(a_{\rm w}-a_{\rm ext})}}{1-\frac{g_{\rm int}}{2\varepsilon_{\rm g}}\frac{1+\bar\zeta_{\rm ext}\tan(a_{\rm w}-a_{\rm ext})\cot(g_{\rm ext}-g_{\rm int})}{\cot(g_{\rm ext}-g_{\rm int})+\zeta_{\rm ext}\tan(a_{\rm w}-a_{\rm ext})}}\\ &=-\frac{A_p}{\varepsilon_{\rm g}}\frac{g_{\rm int}}{b^2}\\ &\quad\times\frac{[1+\bar\zeta_{\rm ext}\tan(a_{\rm w}-a_{\rm ext})][1+\cot(g_{\rm ext}-g_{\rm int})]}{\left\{\begin{array}{l}\cot(g_{\rm ext}-g_{\rm int})+\bar\zeta_{\rm ext}\tan(a_{\rm w}-a_{\rm ext})\\ -\frac{g_{\rm int}}{2\varepsilon_{\rm g}}\left[1+\begin{array}{l}\bar\zeta_{\rm ext}\tan(a_{\rm w}-a_{\rm ext})\\ \times\cot(g_{\rm ext}-g_{\rm int})\end{array}\right]\end{array}\right\}}.\end{aligned} \tag{E7}$$

We assumed the ultrarelativistic limit ($b\to 0$) $K_1(b)\simeq 1/b$ and next we take $g_{\rm int}\gg 1$

$$A = \frac{2A_p}{b^2}\frac{[\cot(a_w - a_{ext}) + \bar{\zeta}_{ext}][1 + \cot(g_{ext} - g_{int})]}{\cot(a_w - a_{ext}) + \bar{\zeta}_{ext}\cot(g_{ext} - g_{int})}. \tag{E8}$$

In Appendix D we show that the relevant resonances occur for

$$\cot(a_w - a_{ext}) = 0 \quad \cot(g_{ext} - g_{int}) = 0. \tag{E9}$$

We conclude that

$$A(\omega \sim \omega_0) \simeq \frac{2\bar{\zeta}_{ext}}{b^2}\frac{A_p}{\cot(a_w - a_{ext}) + \bar{\zeta}_{ext}\cot(g_{ext} - g_{int})} \simeq \frac{-2cF_f\frac{\varepsilon_g}{\varepsilon_r}\sqrt{\frac{1}{\varepsilon_g - 1}}}{(\frac{\omega_0}{\gamma\beta c}R_{int})^2(R_w - R_{ext})}\frac{A_p}{\delta\omega + \frac{\delta\varepsilon F_f\omega_0}{2(\varepsilon_r - 1)}} \tag{E10}$$

and defining $\bar{\omega} \equiv (\omega_0 - \omega)/\Delta\omega$ we find

$$A(\omega \sim \omega_0) \simeq \frac{\frac{2cq\mu_0}{(2\pi)^2}}{(\frac{\omega_0}{\gamma\beta c}R_{int})^2}\frac{F_f\frac{\varepsilon_g}{\varepsilon_r}\sqrt{\frac{1}{\varepsilon_g - 1}}}{(R_w - R_{ext})\Delta\omega} \times \frac{(\bar{\omega} + \frac{j}{2})I_0(\frac{2\pi}{\gamma\beta}\frac{r_\sigma}{\lambda_0})}{\bar{\omega}^2 + \frac{j}{2}\bar{\omega} + \frac{\alpha cF_f}{2\Delta\omega(\varepsilon_r - 1)}}. \tag{E11}$$

The secondary longitudinal electric field is found from

$$E_z^{(sec)}(r, r_\sigma, z, t) = \int_{-\infty}^{\infty} d\omega \exp\left[j\omega\left(t - \frac{z}{v}\right)\right] \times I_0\left(\frac{2\pi}{\gamma\beta}\frac{r}{\lambda_0}\right)\frac{j\omega}{\gamma^2}A(\omega) \tag{E12}$$

and defining radial Green's function $G_r^{(glass)}(r, r_\sigma) \equiv I_0(2\pi r/\gamma\beta\lambda_0)I_0(2\pi r_\sigma/\gamma\beta\lambda_0)$ we have

$$E_z^{(sec)} \equiv E_z^{(sec)}\left(r, r_\sigma, t = \frac{z}{v}\right) = G_r^{(glass)}(r, r_\sigma)\frac{\frac{2cq\mu_0\omega_0}{(2\pi)^2}}{(\frac{\omega_0}{c}R_{int})^2}\frac{F_f\frac{\varepsilon_g}{\varepsilon_r}\sqrt{\frac{1}{\varepsilon_g - 1}}}{(R_w - R_{ext})\Delta\omega} \times \int_{-\infty}^{\infty} d\omega j\frac{\bar{\omega} + j/2}{\bar{\omega}^2 + (j/2)\bar{\omega} + \bar{a}^2}. \tag{E13}$$

The integral in Eq. (E13) may be transformed into form

$$I(\bar{a}) \equiv \int_{-\infty}^{\infty} d\omega j\frac{\bar{\omega} + j/2}{\bar{\omega}^2 + (j/2)\bar{\omega} + \bar{a}^2} = -2\int_0^{\infty} du\frac{-\bar{a}^2/2}{(u^2 + \bar{a}^2)^2 + (u/2)^2}, \tag{E14}$$

where $\bar{a}^2 = \alpha cF_f/2\Delta\omega(\varepsilon_r - 1)$ and then evaluated analytically:

$$I(\bar{a}) = \bar{a}^2\int_0^{\infty} du\frac{1}{(u^2 + \bar{a}^2)^2 + (\frac{u}{2})^2} = \frac{\pi}{\sqrt{1 + 16\bar{a}^2}}. \tag{E15}$$

Thus expression for the secondary electric field is

$$E_z^{(sec)} = \frac{q}{2\pi\varepsilon_0 R_{int}^2}\frac{F_f\frac{\varepsilon_g}{\varepsilon_r}\sqrt{\frac{1}{\varepsilon_g - 1}}}{\frac{\omega_0}{c}(R_w - R_{ext})}\frac{1}{\sqrt{1 + 16\bar{a}^2}} \times I_0\left(\frac{2\pi}{\gamma\beta}\frac{r}{\lambda_0}\right)I_0\left(\frac{2\pi}{\gamma\beta}\frac{r_\sigma}{\lambda_0}\right). \tag{E16}$$

[1] R. Tomás, Phys. Rev. ST Accel. Beams **13**, 014801 (2010).
[2] F. Gao, M. E. Conde, W. Gai, C. Jing, R. Konecny, W. Liu, J. G. Power, T. Wong, and Z. Yusof, Phys. Rev. ST Accel. Beams **11**, 041301 (2008).
[3] S. V. Shchelkunov, T. C. Marshall, G. Sotnikov, J. L. Hirshfield, W. Gai, M. Conde, J. Power, D. Mihalcea, and Z. Yusof, Phys. Rev. ST Accel. Beams **15**, 031301 (2012).
[4] S. Y. Park and J. L. Hirshfield, Phys. Rev. E **62**, 1266 (2000).
[5] X. E. Lin, Phys. Rev. ST Accel. Beams **4**, 051301 (2001).
[6] B. M. Cowan, *Photonic Crystal Laser-Driven Accelerator Structures (prepared for the Department of Energy under Contract No. DE-AC02-76SF00515, available from the National Technical Information Service, U.S. Department of Commerce, 5285 Port Royal Road, Springfield, VA 22161, 2007).*
[7] A. Mizrahi and L. Schächter, Phys. Rev. E **70**, 016505 (2004).
[8] L. Schächter, R. L. Byer, and R. H. Siemann, Phys. Rev. E **68**, 036502 (2003).
[9] E. A. Peralta, K. Soong, R. J. England, E. R. Colby, Z. Wu, B. Montazeri, C. McGuinness, J. McNeur, K. J. Leedle *et al.*, Nature (London) **503**, 91 (2013).
[10] M. Voin and L. Schächter, Phys. Rev. Lett. **112**, 054801 (2014).
[11] The International Linear Collider, Vol. 1, Technical Design Report, 2013.
[12] T. Y. Chang and O. R. Wood, Appl. Phys. Lett. **24**, 182 (1974).
[13] K. Stenersen and G. Wang, Opt. Commun. **39**, 251 (1981).
[14] M. Voin, W. D. Kimura, and L. Schächter, Nucl. Instrum. Methods Phys. Res., Sect. A **740**, 117 (2014).
[15] DLMF, NIST Digital Library of Mathematical Functions, http://dlmf.nist.gov/, release 1.0.9 of 2014-08-29, online companion to [16].
[16] *NIST Handbook of Mathematical Functions*, edited by F. W. J. Olver, D. W. Lozier, R. F. Boisvert, and C. W. Clark (Cambridge University Press, New York, 2010), print companion to [15].
[17] M. N. Polyanskiy, I. V. Pogorelsky, and V. Yakimenko, Opt. Express **19**, 7717 (2011).

[18] D. Haberberger, S. Tochitsky, and C. Joshi, Opt. Express **18**, 17865 (2010).
[19] L. Rothman, I. Gordon, Y. Babikov, A. Barbe, D. C. Benner, P. Bernath, M. Birk, L. Bizzocchi, V. Boudon, L. Brown *et al.*, J. Quant. Spectrosc. Radiat. Transfer **130**, 4 (2013), {HITRAN2012} special issue.
[20] A. E. Siegman, *Lasers* (University Science Books, Sausalito, CA, 1986).
[21] R. H. Pantell and H. E. Putoff, *Fundamentals of Quantum Electronics* (Wiley, New York, 1969).
[22] Z. Toroker, M. Voin, and L. Schächter, High Power Laser Sci. Eng. **2**, e29 (2014).
[23] Z. Toroker and L. Schächter, Phys. Rev. ST Accel. Beams **18**, 071301 (2015).
[24] B. C. Stuart, M. D. Feit, A. M. Rubenchik, B. W. Shore, and M. D. Perry, Phys. Rev. Lett. **74**, 2248 (1995).